

AD653770

---

---

# A STUDY OF THE DYNAMICS OF AN UNTUNED CLOCK MECHANISM

---

---

A REPORT OF WORK CARRIED OUT UNDER TASK  
ASSIGNMENT NO.1 (modified) OF CONTRACT  
CST-1224 FOR THE NATIONAL BUREAU OF  
STANDARDS . . . . .

DOWNGRADED TO UNCLASSIFIED  
BY AUTHORITY OF THE  
COMMANDING OFFICER OF DOFL  
/s/ L. RUBINOWITZ, CHIEF 22.0  
15 DEC. 1953

VIRGINIA MILITARY INSTITUTE  
DEPARTMENT OF PHYSICS  
LEXINGTON, VIRGINIA  
SEPTEMBER 1, 1953

BEST AVAILABLE COPY

ABSTRACT OF REPORT ON THE DYNAMICS OF AN UNTUNED CLOCK MECHANISM

As a first approach to the study of untuned clock mechanisms, the physical behaviour of the verge-star wheel combination of the Lux\* clock mechanism was studied by means of a scaled-up model. Differential equations of motion for the motion were developed and solved. Curves showing typical motions were obtained. The dependence of equilibrium velocities (or equilibrium time delays) upon (1) applied torque, (2) star wheel moment of inertia, (3) verge moment of inertia, was studied. The following empirical equation for time delay per revolution is derived

$$T = B \cdot \tau^{-.5} \cdot I_v^{.612} \cdot I_w^{-.112}$$

B is a constant factor depending probably upon geometrical shapes and distances in the star wheel - verge combination.

Application of the above results to the actual mechanism can be made.

\* Note: The Lux clock was designed by the Raymond Engineering Laboratories of Middletown, Connecticut, and was manufactured for the National Bureau of Standards by the Lux Clock Manufacturing Company of Waterbury, Connecticut.

## I. INTRODUCTION

The Lux clock is a device used in ordnance work as a time delay mechanism. It consists of a spring driven gear train terminated by a gear wheel called the star wheel. The constant applied torque of the spring is transmitted through the gear train to the star wheel where it appears as a constant applied torque of different magnitude. Unless otherwise specified the word "torque" will refer to the torque applied to the star wheel, and the remainder of the gear train as well as the spring will neither be shown in diagrams nor otherwise discussed. The validity of this method will be demonstrated later.

The teeth of this star wheel engage alternately one face and then the other of an oscillating verge. The motion of this verge in turn controls the motion of the star wheel; in particular it determines an upper limit to the mean velocity with which the star wheel can turn.

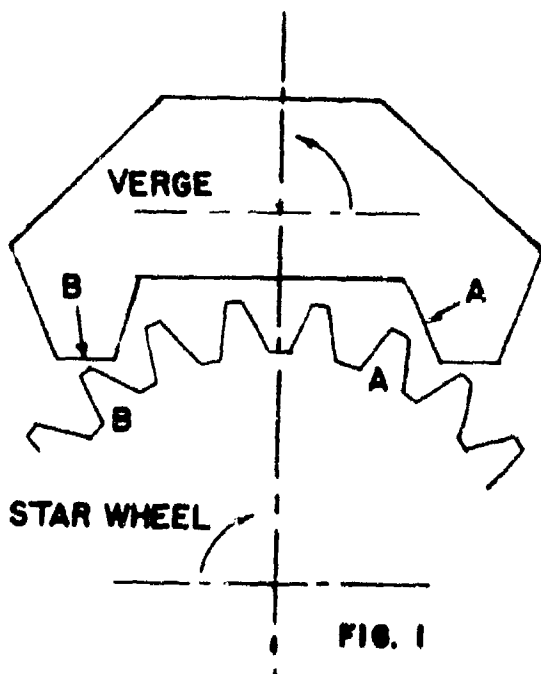


Fig. 1 is a simple sketch of the star wheel verge combination used in the Lux clock. Dimensions will be found on prints Nos. 485-7, 906-47 of the Raymond Engineering Co.

It is assumed throughout this work that the direction of motion of the starwheel in all diagrams is clockwise and that this is the positive sense of rotation of the wheel. As the wheel rotates through one tooth space the verge oscillates counterclockwise then clockwise into its original position. A tooth on the wheel (A) strikes the pallet face A on a leading

collision and presses against the pallet face A during leading contact. Tooth B strikes pallet face B on a trailing collision and during trailing contact. It is our convention that a counterclockwise rotation of the verge shall have a positive sense, a clockwise rotation a negative sense. The arrows on verge and wheel in Fig. 1 show these positive senses.

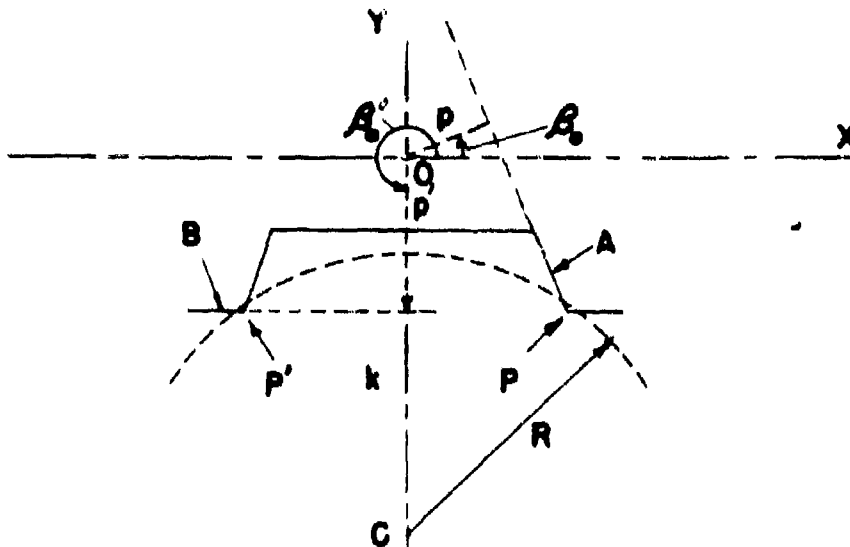
## II. SPACE RELATIONSHIPS

### (A) Verge Position versus Wheel Position

It is of prime importance to know how the position of the verge depends upon the position of the wheel, this completely aside from dynamical considerations. We will find in this section the possible positions of the verge allowed by the wheel under geometrical considerations only. The discussion will also serve to introduce the terminology.

Reference to Fig. 1 is somewhat misleading but an examination of the actual teeth of the star wheel will show that contact between tooth and pallet face occurs very nearly at the point of the tooth rather than over on the tooth face. We assume throughout that contact occurs only at the tooth point.

Before proceeding to the calculations the following point should be noted. (Refer to Fig. 1) As a tooth moves along a pallet face it comes to a position of last contact. As the wheel moves, this tooth (say A) slips free of the verge. Since we are interested in the extreme geometrical positions possible we now imagine the wheel to stop and the verge to move until we have a collision between tooth B and pallet face B. Again the wheel moves, tooth B sliding along pallet face B until its position of last contact is reached. Once more we hold the tooth in place and allow the verge to come around until a (new) tooth A strikes pallet face A. Again wheel moves so that tooth A slides along pallet face A until last contact. It is for the two regions of sliding contact (leading and trailing) that we shall investigate the verge position - wheel position relationship.



VERGE IN EQUILIBRIUM

FIG. 2

Fig. 2 represents the verge in an equilibrium position. This could occur for either leading or trailing case, of course. Certain distances in this diagram are determined from specifications. They are:  $k$  - distance from center of rotation of verge ( $O$ ) to center of rotation of wheel ( $c$ ),  $R$  - radius of circle along which points of rotation of star wheel teeth move. Angles  $\beta_1, \beta_2$  are also known as are the coordinates of  $P$  and  $P'$ . It is clear that point  $o$  serves as the origin for the  $(x, y)$  coordinates.

The equations of the pallet faces can be written in the form

$$x \cos \beta + y \sin \beta = p$$

$p$  in either case can be found by using the known values of  $\beta_0$ ,  $(x, y)$  mentioned above.

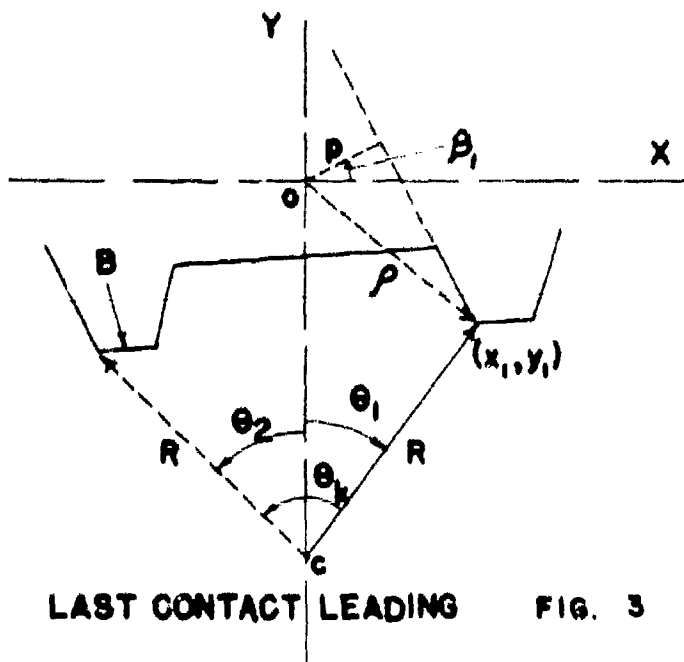


Fig. 3 shows the wheel-verge combination at last contact leading.  $(x_1, y_1)$  are coordinates of the leading verge corner,  $\theta_1$  is the angle measured from the  $y$  axis to the center line of the tooth, designated by  $R$ . An angle such as  $\theta_2$  will be negative.

LAST CONTACT LEADING FIG. 3

We wish to find  $\theta_1$  as the upper limit of  $\theta$  during leading contact.

Equation of pallet face:  $x \cos \beta + y \sin \beta = p$  (1)

$$x = R \sin \theta$$

Equation of tooth circle:  $y = k + R \cos \theta$  (2)



Now we have found extreme positions of verge during leading contact ( $B_2, B_1$ ) and the corresponding wheel positions ( $\theta_2, \theta_1$ ).

Any desired points between these extremes can be determined from equation (3). Similar results hold for trailing contact. While the angles is satisfactory for locating wheel positions  $B, B'$  are not satisfactory for locating verge positions. We adopt a new angle  $\alpha$ , which will represent the displacement of the verge from its equilibrium position.  $\alpha > 0$  if the displacement is counterclockwise, and  $\alpha < 0$  if the displacement is clockwise.  $\alpha$  can be found from the known values of  $B$  or  $B'$  and simple geometrical considerations.

The results of such calculations are displayed in the two graphs marked Fig. 5 and Fig. 6. It is to be noted that each of these curves can be reasonably approximated by a straight line, the equation being written on the graph.

It will be noted that these approximations are poor in the regions of larger values of  $\alpha$ . However it is just this region into which the verge never moves when in actual operation. These regions represent possible space positions which are not occupied in the actual operating cycle. Hence in the regions of physical importance the linear approximations are fairly accurate.

Fig-13

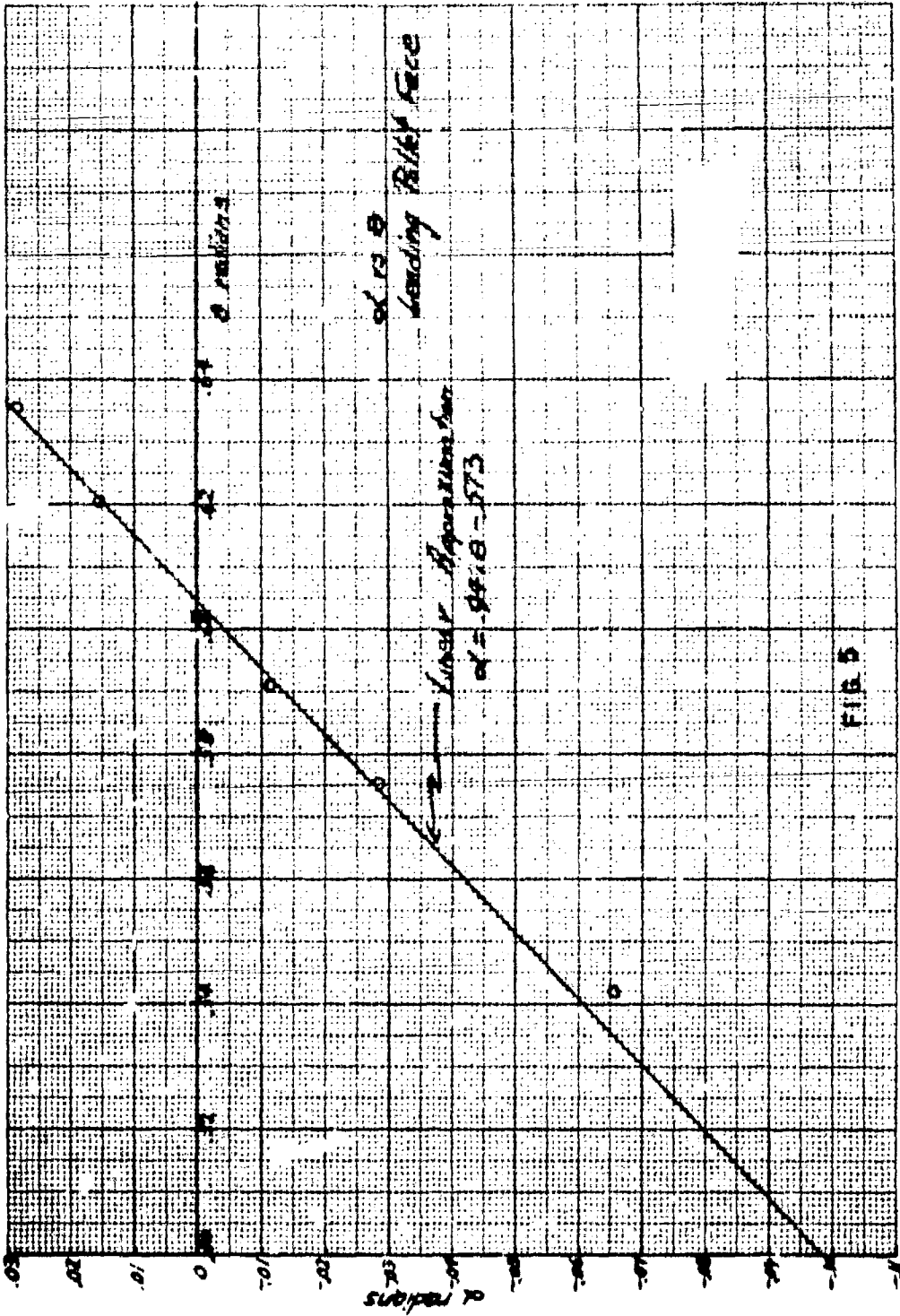
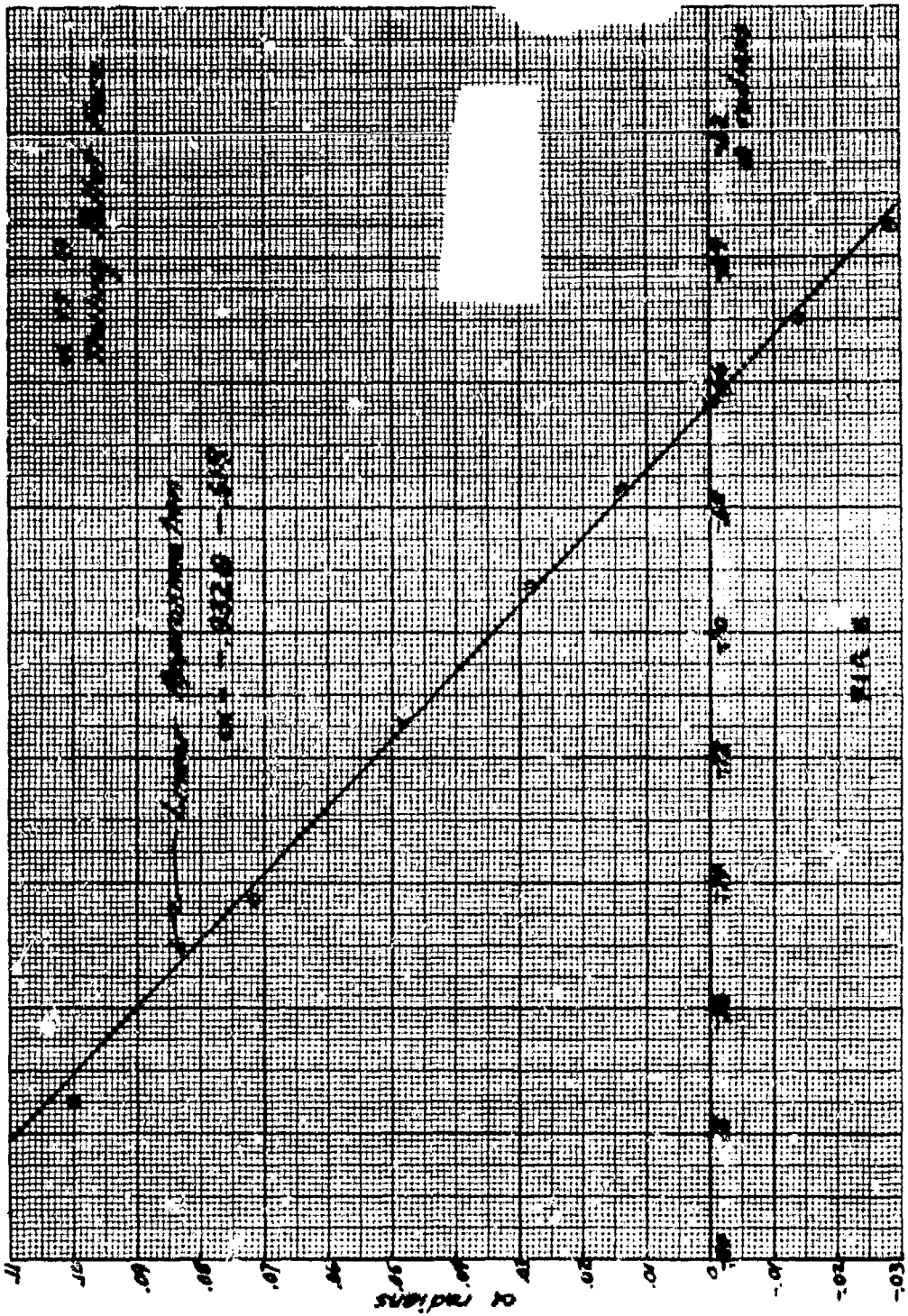


FIG 5



(B) Lever Arm Ratio versus Wheel Position

It will become necessary later to make use of a second geometrical relationship which we next describe. We consider the leading case.

**TOPQUES - LEADING CONTACT**

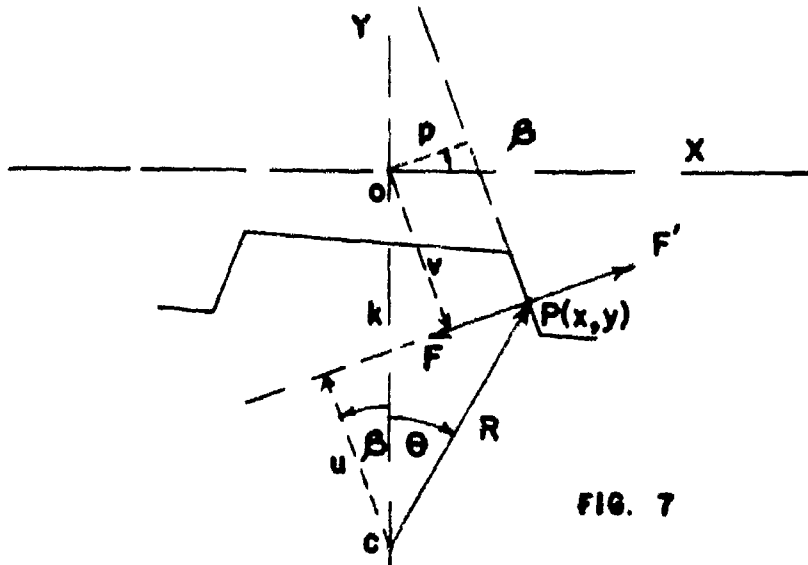


FIG. 7

Fig. 7 shows the action and reaction forces between verge and wheel. The distance  $u$  and  $v$  will be lever arms of the torques applied to wheel and verge respectively by  $F$  and  $F'$ , normal to pallet face.

Inspection of the figure shows that  $u = R \cos (\theta + \beta)$ .

Let the coordinates of  $P$  be  $(x, y)$ . Then we can write

$$v = \sqrt{(x^2 + y^2) - p^2}$$

But  $x = R \sin \theta$ ,  $y = k + R \cos \theta$  ( $k < 0$ )

So  $v = \sqrt{R^2 + k^2 - p^2} + 2kR \cos \theta$  ( $k < 0$ ).

Now for the various values of  $\theta$  in the range of leading contact, already determined for the  $\alpha$  vs.  $\theta$  relationship, we compute  $u$ ,

v, and u/v, plotting against  $\theta$ . The results are given on the graph marked Fig. 8.

The trailing case may be handled in an identical way and its results are plotted on the graph marked Fig. 9.

In each case it is found possible to approximate the u/v vs.  $\theta$  relationship reasonably well with a linear function, called general

$$\frac{u}{v} = F_1 \theta + G.$$

These results will be used later.

Fig-13

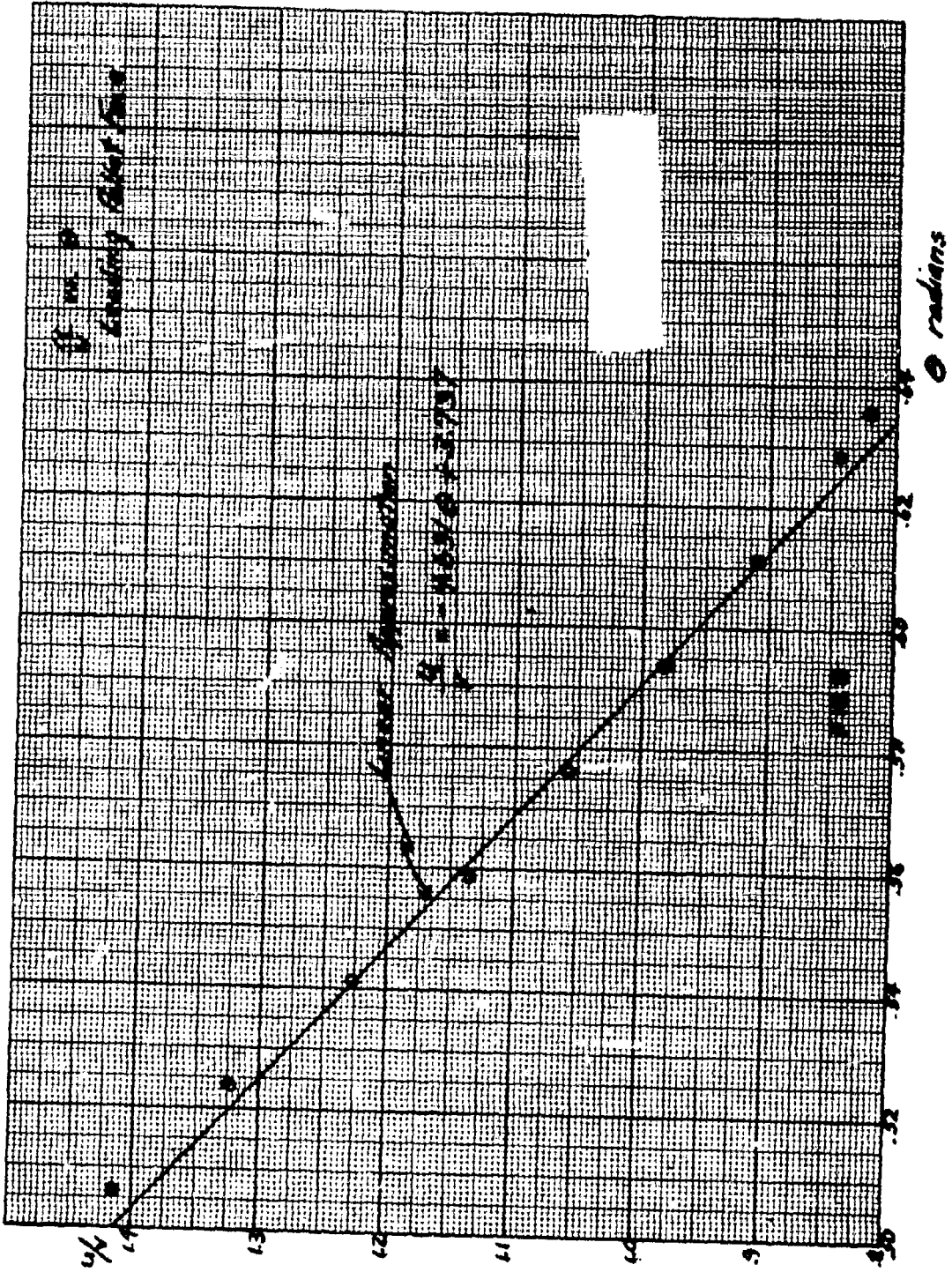
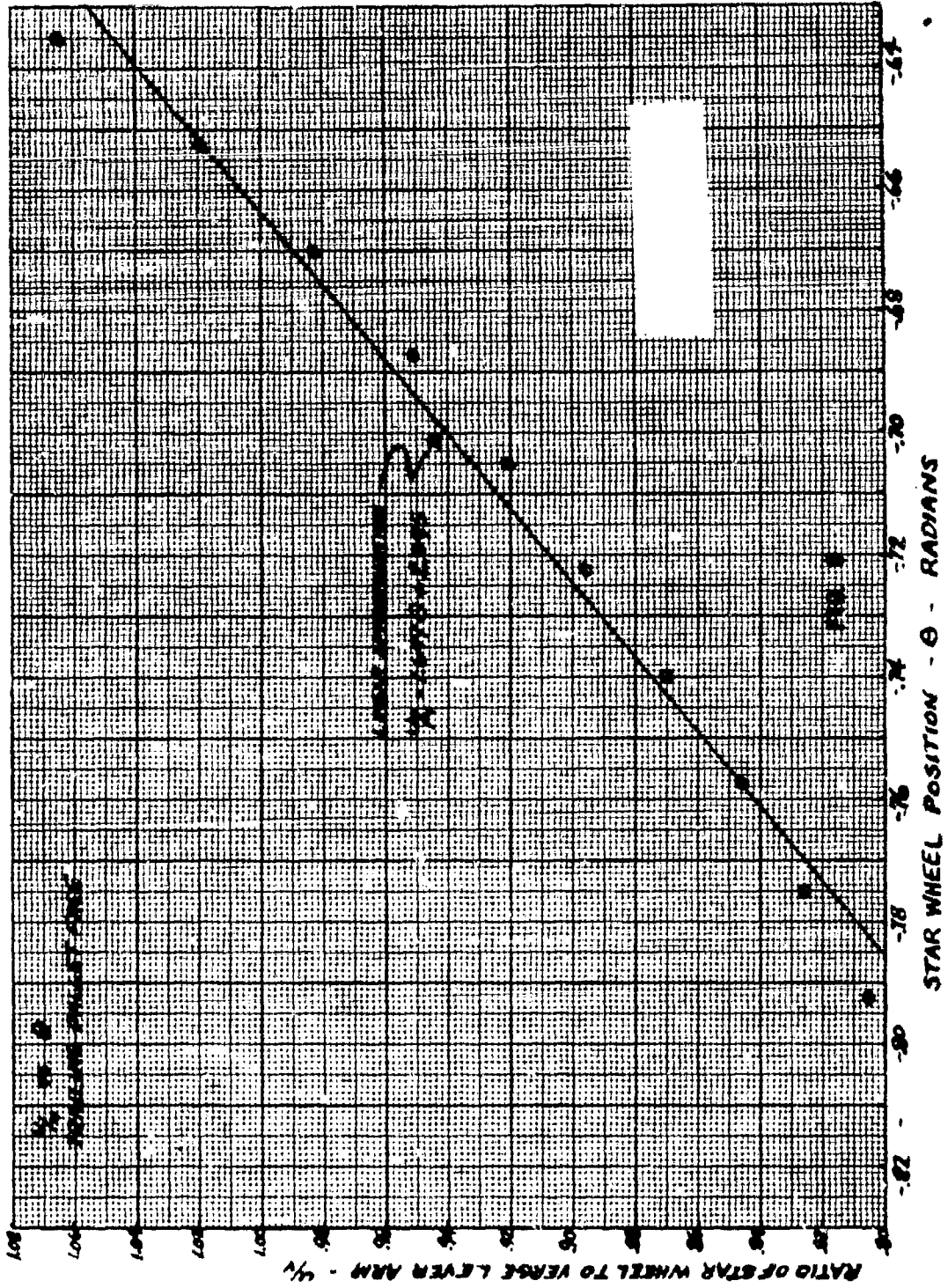


Fig-13



### III. QUALITATIVE DISCUSSION OF MECHANISM BEHAVIOUR

Superficial observation of the mechanism shows that the effect of the verge upon the wheel is in general as follows.

(1) The wheel rotates in leading contact with verge, accelerating the verge up to the point of last contact. During this period potential energy of the spring is being converted into kinetic energy of the wheel-verge system.

(2) After last contact leading there is a period of free motion, in that the verge and wheel are temporarily free of each other. During this period the wheel continues to accelerate under the applied torque while the verge rotates at constant speed.

(3) After a short interval the trailing collision occurs, at some point on the curve of Fig. 6. As a result of this collision some kinetic energy is lost from the wheel-verge system and is transformed into heat. This means that the velocities of wheel and verge are changed. In general the effect of the collision is to slow down the wheel and reverse (or at least stop) the motion of the verge.

(4) Now the wheel accelerates once more, driven by the gear train and spring, and, pushing the verge before it, accelerates up to the point of last contact trailing.

(5) After last contact trailing a free period occurs once more, during which the wheel accelerates and the verge moves uniformly.

(6) After a short interval leading collision occurs. Note that the tooth now involved in leading collision and leading contact is not that referred to in paragraph (1) above but is the next succeeding tooth on the wheel. As in trailing collision energy is lost by wheel and verge, and their velocities are changed.

(7) Finally wheel and verge once more accelerate in leading contact until last contact leading occurs, and the cycle begins to repeat.

To put the matter as succinctly as possible we say this: during one tooth space advance of the wheel (which is one cycle of the verge) a certain amount of energy is fed into the wheel-verge system because of the constant torque applied to the wheel. But during this time energy is lost by the wheel-verge combination in the two collisions. If energy gain and energy loss are equal, then the mechanism has reached a true cyclic condition where the entire sequence of events is repeated each cycle with the same values of velocity, acceleration, angular displacement, etc. This we call

the terminal condition of the apparatus. This terminal condition is not attained instantaneously upon release of the mechanism from rest. Several cycles of the verge will be required before it is attained.

IV. QUANTITATIVE DISCUSSION OF MECHANISM BEHAVIOUR

In this section we derive the basic equations for predicting the behaviour of the mechanism.

(A) Leading and trailing contact

(1) Leading contact. - Reference should be made to Fig. 7. The forces  $F$ ,  $F'$  are the forces of action and reaction on tooth and verge. It is assumed that these forces are normal to the pallet face; that, in other words, there is no frictional force between verge and tooth. This will be our basic assumption. The figure shows that situation for any point of leading contact.

The force  $F$  is a force exerted on the wheel (on the tooth denoted by  $R$ ) and results in a torque of magnitude  $F \cdot u = Fu$  on the wheel. The moment of inertia of the wheel is  $I_w$ . There is also exerted on the wheel a constant torque  $\tau$ , originating at the spring and transmitted to the star wheel by the gear train. Hence we write

$$\tau - \tau(\theta) - I_w \frac{d^2\theta}{dt^2} = I_w \ddot{\theta}$$

as the differential equation of motion of the wheel.

For the verge, the only torque is  $\tau'(\theta) = F'v$ , and this torque tends to accelerate the verge, in the positive sense, in accordance with our initial assumptions. Hence we write

$$+ \tau'(\theta) - I_v \frac{d^2\alpha}{dt^2} = I_v \ddot{\alpha}$$

as the differential equation of motion of the verge.

Collecting equations we have

$$\tau - \tau(\theta) - \tau - F \cdot u = I_w \ddot{\theta}$$

$$\tau'(\theta) - F' \cdot v = I_v \ddot{\alpha}$$

which can be written as

$$- \frac{F}{F'} \cdot \frac{u}{v} = \frac{I_w \ddot{\theta} - \tau}{I_v \ddot{\alpha}}$$

Of course  $F = F'$  in magnitude, so

$$- \frac{u}{v} = \frac{I_w \ddot{\theta} - \tau}{I_v \ddot{\alpha}} \quad (I)$$

(2) Trailing contact

By similar considerations we can show that on trailing contact we have an equation

$$\frac{u}{v} = \frac{I_L \ddot{\theta} - \tau}{I_V \ddot{\alpha}} \quad (II)$$

(3) Solution of Differential Equations

(I) and (II) cannot be solved without further simplification. First remember that for either leading or trailing case we have been able to write  $\alpha = \gamma \theta + D$ ,  $\gamma$  and  $D$  being known in each case. It follows at once that

$$\ddot{\alpha} = \gamma \ddot{\theta}$$

Secondly we can now make use of the fact that we can write  $\frac{u}{v} = F \cdot \theta + G$  where  $F$ ,  $G$  are known constants in both leading and trailing cases.

At once we see that we can simplify (I) and (II) as follows

$$(I) \quad -\frac{u}{v} = \frac{I_L \ddot{\theta} - \tau}{I_V \alpha}$$

$$-(F \cdot \theta + G) = \frac{I_L \ddot{\theta} - \tau}{I_V \gamma \theta}$$

which becomes

$$\ddot{\theta} = \frac{\tau}{A\theta + B} \quad \begin{array}{l} A = F I_V \gamma \\ B = G I_V \gamma + I_W \end{array}$$

A first integral is

$$\dot{\theta}^2 = \dot{\theta}_0^2 + \frac{2\tau}{A} \ln \frac{A\theta + B}{A\theta_0 + B}$$

where  $\dot{\theta} = \dot{\theta}_0$  when  $\theta = \theta_0$

Identical considerations lead to a similar solution for the trailing case (to be exhibited later).

A second integral is not possible, so that for some desired information graphical integration must be resorted to.

### (B) Free Motion

This occurs during the small periods of time just following last contact leading and last contact trailing. The verge, which has no torque applied to it during a free period, simply moves with the (constant) speed imparted to it at last contact. The wheel on the other hand is moving under the influence of the constant applied torque, so accelerates uniformly, according to the law

$$\theta = \frac{\tau}{2I_w} t^2 + \dot{\theta}_0 t + \theta_0$$

where  $\dot{\theta} = \dot{\theta}_0$ ,  $\theta = \theta_0$  at  $t = 0$  (This point is usually chosen to be last contact. The situation is more fully described later.)

### (3) Collision

This is the most difficult portion of the cycle to deal with accurately. First we must recognize that there are two unknown quantities for which certain assumptions must of necessity be made. The first is the duration of the impact, the time over which the impulsive torque of collision is being exerted. The second is the degree of elasticity of the impact.

Let us discuss this latter situation first. It is clear that the collisions could not be perfectly elastic, for if they were there could not be the loss of energy which is essential to the behaviour of the mechanism. If the collision is completely inelastic, the mathematical problem is simplified, but it seems somewhat unlikely that this could be true. The collision is most likely to be partially elastic. There is energy lost per collision, but not as much lost as would occur in the completely inelastic case.

If we wish to work with the partially elastic case a number of questions at once confront us, chief of which is the value we should choose for the coefficient of restitution. Next we must assume that the impact time is so small that the effect of the constant torque may be neglected. Then using the conservation laws we could solve for velocities of verge and wheel after collision. There now arises the question of whether the verge and wheel are in contact after collision. If they are not, does the wheel catch up with the verge before position of last contact or not? To answer these questions would not be easy, and the answers themselves would depend largely upon assumptions.

Now if one examines carefully the behaviour of the mechanism during operation, the polishing of the pallet faces seems to indicate that there is contact between verge and tooth at all times following collision. In this respect the collision is apparently inelastic. It is believed that this is not physically an inelastic collision, but that the combination of a finite impact time and the constant applied torque on the wheel produce what is effectively the same thing.

As a result then of our lack of information about physical quantities plus our observation of the mechanism behaviour we decided to proceed on the assumption that the collision was perfectly inelastic and that the impact time was zero. Comparison of theoretical and experimental results will justify this assumption, as we see later.

We shall work out the equations for a leading collision, assumed inelastic with zero time of impact.

There will be exerted on the wheel at impact an impulsive torque only, because the impulse applied by the constant torque is zero if impact time is zero. The law of conservation of angular momentum gives us for the wheel

$$\int \overline{\tau_w} dt = I_w (\dot{\theta} - \dot{\theta}_0) \quad \text{where we deal with vectors throughout.}$$

for the verge

$$\int \overline{\tau_v} dt = I_v (\dot{\alpha} - \dot{\alpha}_0).$$

Now these two torques are not equal in magnitude as a reference to the discussion of the ratio  $u/v$  will show. The impulsive torque

$\int \overline{\tau_w} dt$  is negative in sense, and  $\int \overline{\tau_v} dt$  is positive and it is obvious that the ratio of these integrals is then given by

$$\frac{\int \overline{\tau_w} dt}{\int \overline{\tau_v} dt} = - \frac{u}{v}$$

At leading collision  $\dot{\theta}_0 > 0$  (velocity of wheel before collision)

$\dot{\alpha}_0 < 0$  (velocity of verge before collision)

Now after collision  $\dot{\alpha} - \gamma \dot{\theta} > 0$        $\gamma > 0$

Therefore we write

$$\begin{aligned} I_w (\dot{\theta} - \dot{\theta}_0) &= I_w \dot{\theta} - I_w \dot{\theta}_0 && \text{These terms are no} \\ I_v (\dot{\alpha} - \dot{\alpha}_0) &= I_v \gamma \dot{\theta} - I_v \dot{\alpha}_0 && \text{longer vectors. Signs} \\ &&& \text{attached to numerical} \\ &&& \text{values as indicated above will preserve vector relationships.} \end{aligned}$$

Forming a ratio we have

$$-\frac{u}{v} = \frac{I_w \dot{\theta} - I_w \dot{\theta}_0}{I_v \gamma \dot{\theta} - I_v \alpha_0}$$

We set  $\dot{\theta} = K$  and get

$$\dot{\theta} = \frac{I_w \dot{\theta}_0 + K I_v \alpha_0}{I_w + K I_v \gamma}$$

where  $\dot{\theta}_0 < 0$   
 $\dot{\theta}_0 > 0$   
 $\gamma > 0$

In an analogous manner we can get

$$\dot{\theta} = \frac{I_w \dot{\theta}_0 - K I_v \alpha_0}{I_w - K I_v \gamma'}$$

where  $\dot{\theta}_0 > 0$   
 $\dot{\theta}_0 > 0$   
 $\gamma' < 0$

for trailing collision.

For convenience we assemble all equations below

Contact Leading

$$\dot{\theta}^2 = \dot{\theta}_0^2 + \frac{2\tau}{A} \ln \frac{A\dot{\theta} + B}{A\dot{\theta}_0 + B}$$

$\tau$  = applied torque

$$A = F I_v \gamma$$

$$B = G I_v \gamma + I_w$$

where  $\alpha = \gamma \dot{\theta} + D$

$$\frac{u}{v} = F \dot{\theta} + G$$

Contact Trailing

$$\dot{\theta}^2 = \dot{\theta}_0^2 + \frac{2\tau}{A'} \ln \frac{A'\dot{\theta} + B'}{A'\dot{\theta}_0 + B'}$$

$\tau$  = applied torque

$$A' = F' I_v \gamma'$$

$$B' = G' I_v \gamma' + I_w$$

where  $\alpha' = \gamma' \dot{\theta} + D'$

$$\frac{u'}{v'} = F' \dot{\theta} + G'$$

Free Motion

$$\dot{\theta} = \frac{\tau}{2I_w} t^2 + \dot{\theta}_0 t + \theta_0$$

Collision Leading

$$\dot{\theta} = \frac{I_w \dot{\theta}_0 + K I_v \alpha_0}{I_w + K I_v \gamma}$$

where

$$K = \frac{u}{v} = F \dot{\theta} + G$$

evaluated at the collision angle.

Collision Trailing

$$\dot{\theta} = \frac{I_w \dot{\theta}_0 - K I_v \alpha_0}{I_w - K I_v \gamma'}$$

where

$$K' = \frac{u'}{v'} = F' \dot{\theta} + G'$$

evaluated at the collision angle.

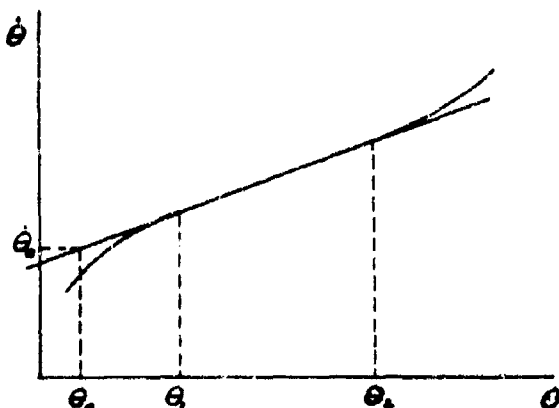
V. SOLUTION OF THE EQUATIONS OF MOTION

The solution of the equations listed above is very long and uninteresting. A complete discussion of the problem including a definition of all terms and symbols is given in Appendix A. Also in Appendix B is a description of a shorter method of solution.

In general we begin the solution by assuming that the system is at rest in a position of leading equilibrium. The wheel is released, begins to move and its velocity (and that of the verge) is computed for several points around the cycle. This process is continued until all values of velocity for a given cycle are repeated in the following cycle. The system has now reached an equilibrium situation which will be repeated each cycle thereafter.

After such a solution has been completed we have a curve on which wheel velocity,  $\dot{\theta}$ , is plotted against wheel position,  $\theta'$ ; and a second curve on which verge velocity,  $\dot{\alpha}$ , is plotted against wheel position,  $\theta'$ . There are two things in which we are most interested. (1) the mean velocity of the wheel from which we get the period of revolution, (2) the relationship of wheel position and time, of verge position and time. These latter curves, if obtainable, can be checked against experimental curves.

We first consider the curve  $\dot{\theta}$  vs.  $\theta'$ . see Fig. 10. This curve is computed for a set of values of  $I_w, I_v, \tau$  to be discussed later. We first assume the curve to be divided into a number of linear segments each of which is represented by an equation



$$\dot{\theta} = K (\theta - \theta_0) + \dot{\theta}_0$$

$$\dot{\theta} = K \theta + A, A = -K \theta_0 + \dot{\theta}_0 \quad (1)$$

The limits of the segment of the curve are  $\theta_1, \theta_2$  as indicated in Fig. 12.

Fig. 12.



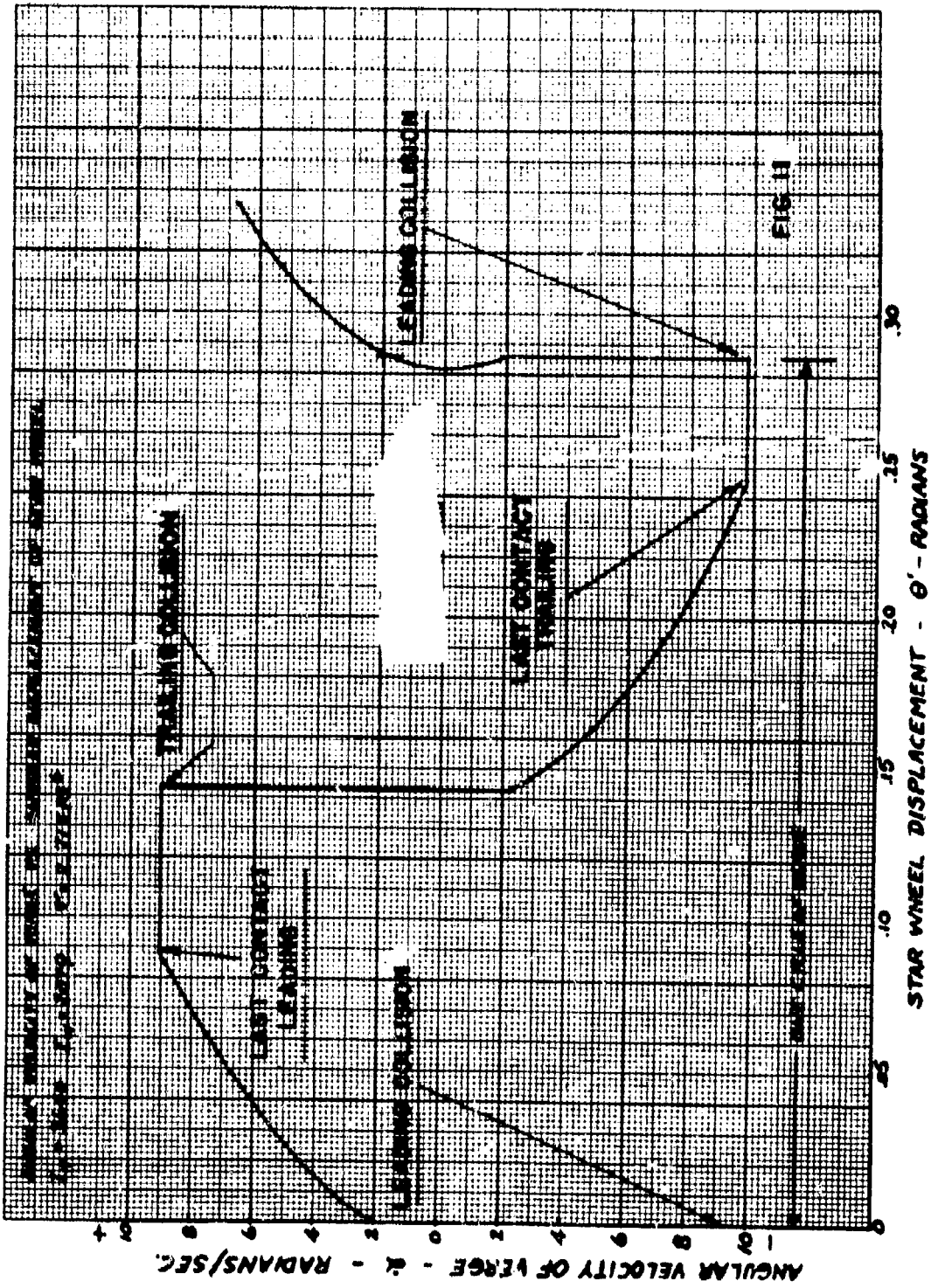


FIG. II

STAR WHEEL DISPLACEMENT -  $\theta$  - RADIANS

ANGULAR VELOCITY OF VERGE -  $\alpha$  - RADIANS/SEC.

It is a simple matter to show that  $\dot{\theta} = \dot{\theta}(\theta)$  as given above, becomes

$$\frac{K\theta + A}{K\theta_0 + A} = e^{K(t - t_0)} \quad (2)$$

when integrated to get  $\theta = \theta(t)$ , and that from this

$$\dot{\theta} = (K\theta_0 + A) e^{K(t - t_0)} \quad (3)$$

The average velocity with respect to time is given by

$$\bar{\dot{\theta}}_t = \frac{\int \dot{\theta} dt}{\Delta t} = \frac{\int (K\theta_0 + A) e^{K(t - t_0)} dt}{\Delta t} = \frac{\theta_2 - \theta_1}{\Delta t}$$

Taking logarithms of (2) and substituting gives

$$\bar{\dot{\theta}}_t = \frac{K(\theta_2 - \theta_1)}{1 - \frac{K\theta_2 + A}{K\theta_1 + A}} \quad (4)$$

From this equation  $\bar{\dot{\theta}}_t$  is computed. This however is a lengthy process for nearly all the curves  $\dot{\theta}$  vs.  $\theta$ , since it requires that we determine  $K$  and  $A$  for each line segment into which the curve is broken.

Let us compute the average velocity  $\bar{\dot{\theta}}_o$  with respect to position rather than with respect to time.

$$\bar{\dot{\theta}}_o = \frac{\int \dot{\theta} d\theta}{\Delta \theta} = \frac{\int (K\theta + A) d\theta}{\Delta \theta}$$

$$\text{or } \bar{\dot{\theta}}_o = \frac{\dot{\theta}_2 + \dot{\theta}_1}{2} = \frac{K(\theta_2 + \theta_1)}{2} + A \quad (5)$$

Returning to equation (4), the logarithm term may be expanded in a series, giving

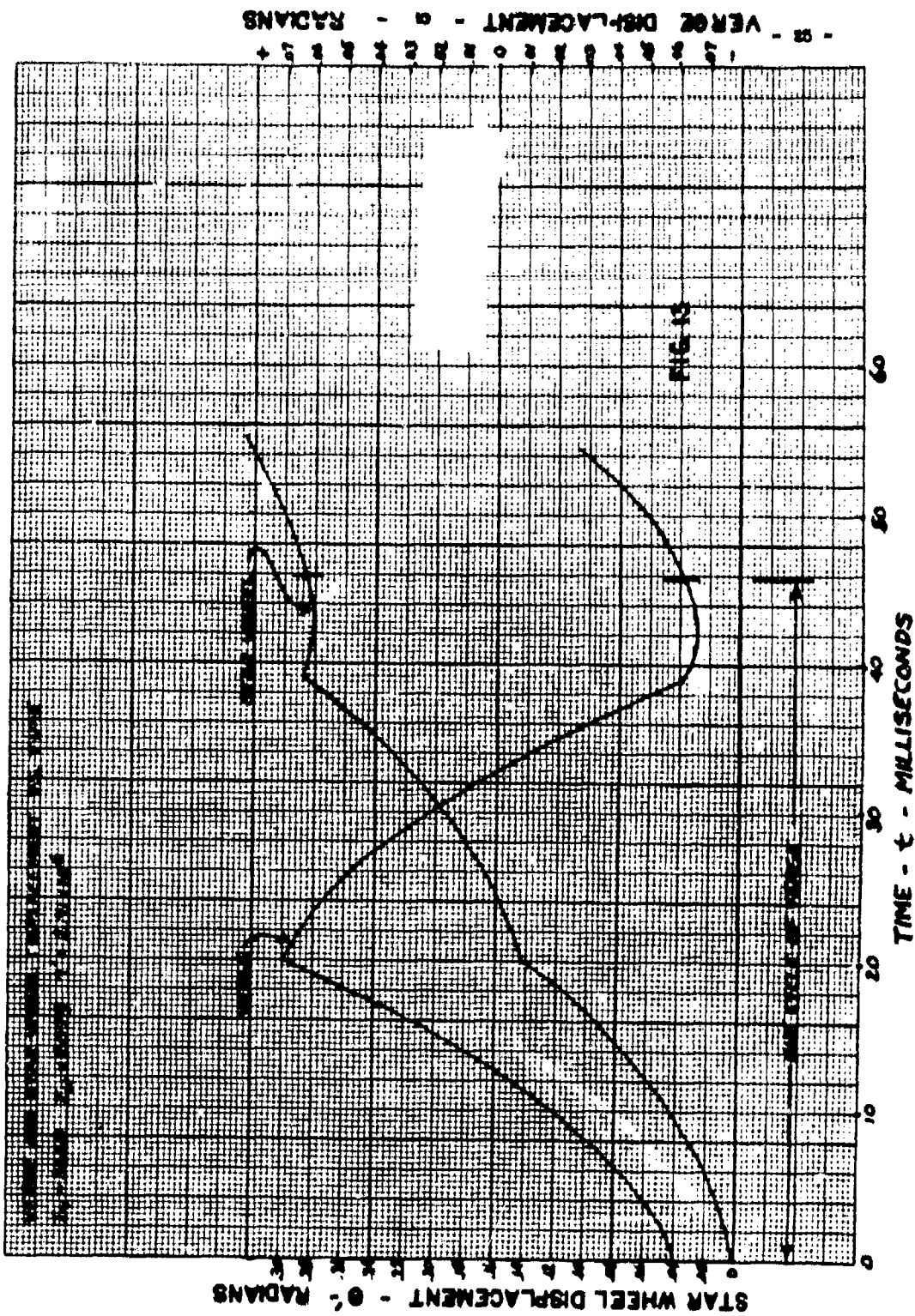
$$\bar{\dot{\theta}}_t = \frac{K\theta_1 + A}{1 - \frac{\Delta \theta}{2(\theta_1 + A/K)} + \frac{\Delta \theta^2}{3(\theta_1 + A/K)^2} - \dots} \quad (6)$$

It can be shown very easily that if  $\frac{\Delta \theta}{(\theta_1 + A/K)} \ll 1$

then equation (6) and equation (5) become identical, and  $\bar{\dot{\theta}}_o = \bar{\dot{\theta}}_t$ . It is much easier to find  $\bar{\dot{\theta}}_o$  from the curve of Fig. 10 than it is to find  $\bar{\dot{\theta}}_t$ , and if  $\Delta \theta = 0.01$  radians, the difference between the values is very small. For this reason the average value,  $\bar{\theta}$ , over any small approximately linear segment of the curve is determined from the expression  $\bar{\theta} = \frac{\theta_2 + \theta_1}{2}$

The angle of rotation of the wheel for one cycle of the verge was divided into small intervals and the average velocity over each of these intervals was read from the graph. The time required for the star wheel to traverse each of these increments was found by dividing the length of the interval by the average velocity for that increment. The sum of these times is the time required for the wheel to turn through the angle of one tooth space, and the delay time per revolution is the sum of these times multiplied by the number of teeth on the star wheel. The average angular velocity of the star wheel ( sometimes called the terminal velocity) is the angle subtended by one tooth space divided by the sum of the time intervals.

From the values of time and the corresponding values of star wheel position a graph of star wheel position versus time can be plotted. Also, since the verge position is known as a function of star wheel position a similar curve of verge position versus time can be plotted. The curves of positions as a function of time for a typical star wheel and verge, shown in Fig. 13, were obtained by this method from the curve of Fig. 10.



VI. DATA, THEORETICAL AND EXPERIMENTAL; THE MODEL

Certain theoretical predictions can be checked experimentally, and wherever this could be done the comparison was made. All results discussed in this section were obtained on the basis of the verge-wheel model described in Section VII - EXPERIMENTAL METHODS. All experimental methods used in obtaining results quoted below are fully described in Section VII.

(A) WHEEL AND VERGE MOTION

As described in the preceding paragraph we were able to obtain curves showing how star wheel position varied with time, and the same for the verge. For the particular case ( $I_v = 3640 \text{ gm. cm.}^2$ ,  $I_w = 2079 \text{ gm cm}^2$ ,  $\tau = 2.71 \times 10^6 \text{ dyne cm.}$ ), we obtained experimental curves by the potentiometer method. Little detail is noted in Fig. 14, which gives star wheel position versus time. General characteristics may be compared with Fig. 13. Fig. 15 shows one of the points of collision magnified by shortening the sweep time. The short straight line segments in each curve represent the effect of the individual windings on the potentiometer.



Fig. 14



Fig. 15

A better comparison of theory versus experiment can be obtained by considering Fig. 16, and Fig. 17.



Fig. 16



Fig. 17

Fig. 16 represents an experimental graph of verge position versus time, obtained by the potentiometer method. The ripples impressed on the curve are not understood. They may represent

simply a vibration of the verge set up, during a collision, and this seems to be the most logical conclusion. Note the excellent general agreement in shape of the curves of Fig. 15 and Fig. 16.

Fig. 17 represents an experimental graph of star wheel position versus time. It was obtained by the photo cell method. It should be noted that if the wheel moves with uniform speed, the trace is triangular in shape. In Fig. 17 this second leg of the triangular trace is showing up. At the four centimeter mark on the left of the curve shows a collision, as it does also at about the 1 centimeter mark. Of course our curve indicates clearly that these collisions are not instantaneous as is the assumption for the curve of Fig. 13. Nevertheless, the general characteristics of theoretical and experimental curves are in good agreement.

Some seven curves like Fig. 13 were obtained theoretically, each for a different torque or moment of inertia. Also there were obtained several other experimental curves like Figs. 16 and 17. In all cases comparison showed reasonable agreement in the general structure of the curves.

#### (B) NUMBER OF CYCLES BEFORE EQUILIBRIUM

In all cases computed as mentioned above it was found that by the fourth cycle of motion equilibrium had been established.

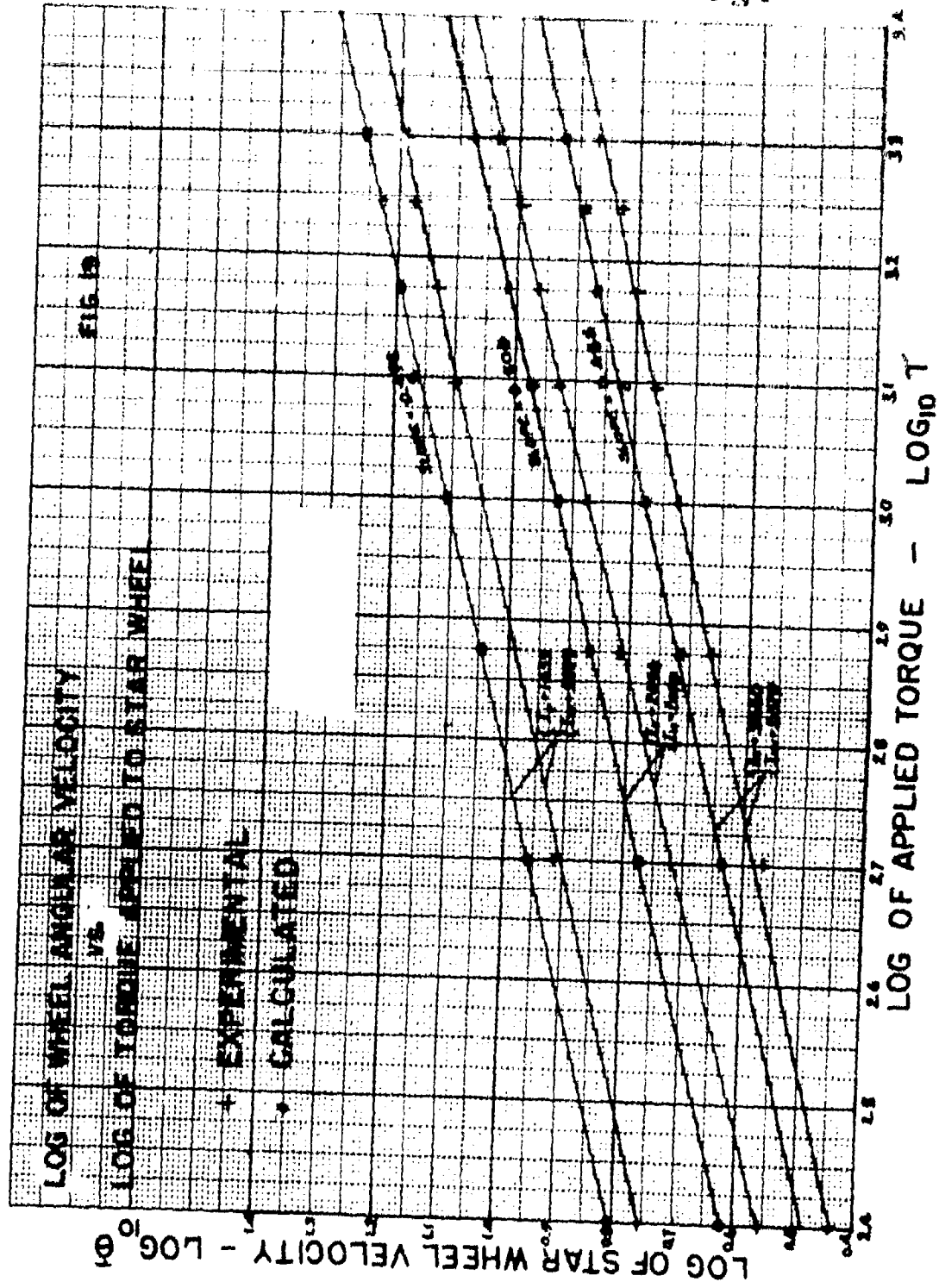
No particularly striking experimental evidence was obtained by the method of Section VII part (C), and no photographs are included. Such small evidence as we have indicates with certainty that equilibrium is established within four cycles.

#### (C) VARIATION OF TERMINAL VELOCITY WITH APPLIED TORQUE

By the "terminal velocity" we mean the average or mean velocity over a cycle after equilibrium has been reached. This was computed as explained in preceding Section V from curve in Fig. 10. For each new choice of torque ( $I_v$ ,  $I_w$  unchanged) a new value of terminal velocity is computed, using one of the methods outlined in Appendix A or Appendix B. Fig. 18 is a graph of  $\bar{\theta}$  vs.  $\tau$ . Three curves are drawn, one for each of three values of  $I_v$ ;  $I_w$  being unchanged in all cases. Both experimental and theoretical points are plotted. In Fig. 19 the same data appears, now plotted as  $\log \bar{\theta}$  vs.  $\log \tau$ . Measurements of the slope of these curves (both experimental and theoretical) give a value very close to 0.5. This means of course that

$$\bar{\theta} \sim \tau^{1/2}$$





A cursory inspection of the equations used (Appendix A or Appendix B) indicate that this relationship is to be expected. The fact that we do find it true experimentally is further evidence of the validity of the assumptions used in our theoretical reasoning.

(D) VARIATION OF TERMINAL VELOCITY WITH  $I_v$ .

On Fig. 20 are plotted several curves,  $\bar{\theta}$  vs.  $I_v$ . Three such curves are given, each being taken at a different torque, but  $I_w$  being constant for all. Both the experimental and the theoretical curves are plotted in each case. Fig. 21 exhibits the same data, plotted as  $\log \bar{\theta}$  vs.  $\log I_v$ . It is noticeable here that the  $\log - \log$  plots are straight lines, with an average slope of  $-.612$ . This indicates that

$$\bar{\theta} \sim I_v^{-.612}$$

is the functional dependence of  $\bar{\theta}$  on  $I_v$ . There is no obvious way in which this dependence can be predicted by theory.

(E) VARIATION OF TERMINAL VELOCITY WITH  $I_w$ .

The agreement of theoretical and experimental results for variable  $I_w$  was poor. In general, theory predicts that as  $I_w$  increases, terminal velocity remains nearly constant. Fig. 22 shows this at three different values of  $I_v$ ,  $\tau$  being held constant in all cases at  $\tau = 2.71 \times 10^6$  dyne cms. Only three points on each curve were obtained experimentally and these are plotted. For the two upper curves at least, very poor agreement will be noted. Fig. 23, is a plot of experimental values only. The points occur in families of three members, each member of the family being characterized by a different value of  $I_w$ . An examination of these points will help convince one that the effect of  $I_w$  on  $\bar{\theta}$  is small indeed. In fact the scatter of the experimental points hides completely any dependence which may exist. It is of interest to note that at the point where  $I_v = 2598$ , regardless of the value of  $I_w$ , the three values of  $\bar{\theta}$  in any one family of curves nearly coincide. Why this should occur is not known. One curve has been drawn for each group of points as an aid to picking out the groups.

In general we find it difficult to draw conclusions regarding the dependence of  $\bar{\theta}$  on  $I_w$ . We shall determine this dependence in a different way.



Fig-13

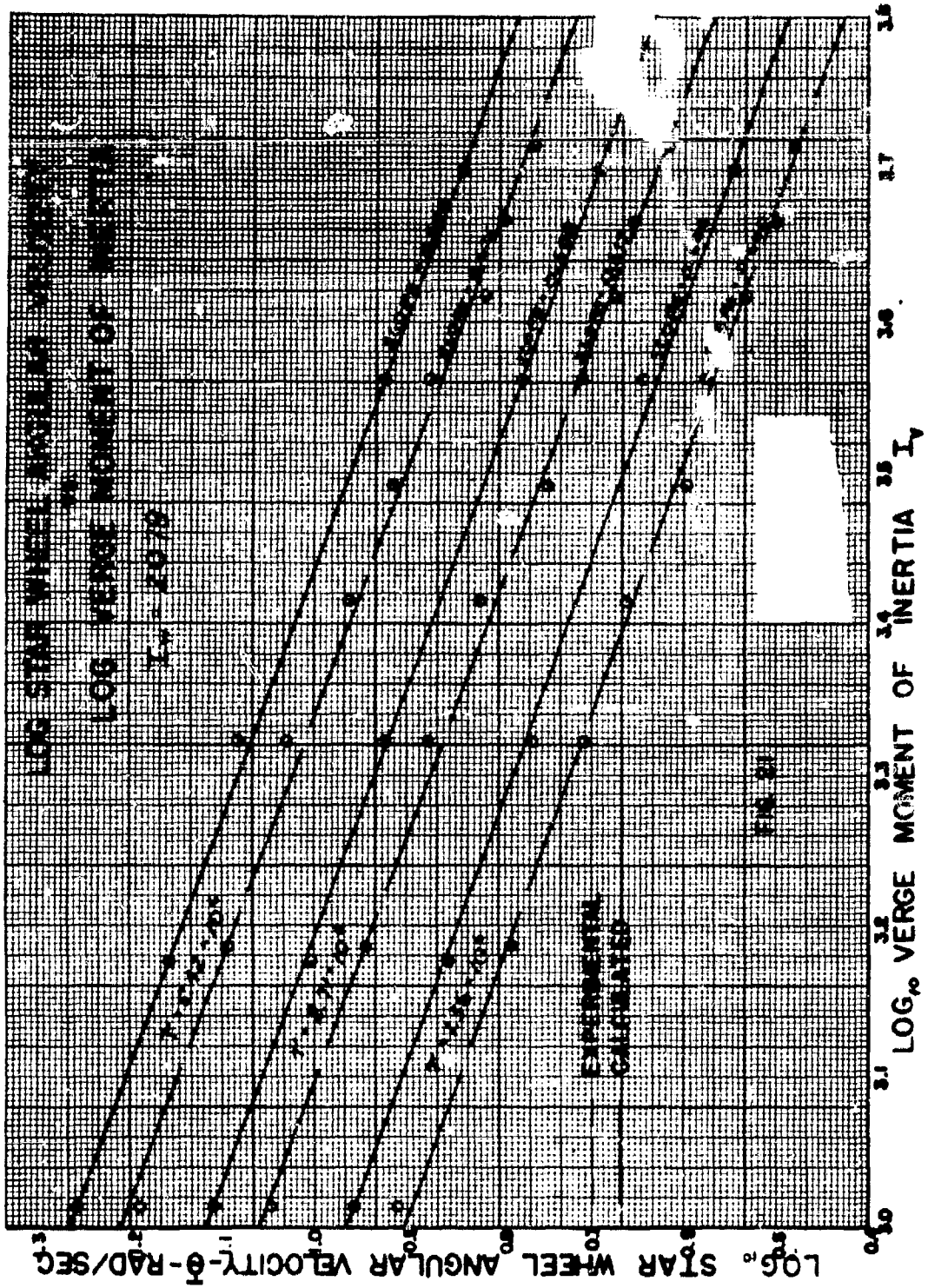


Fig-13

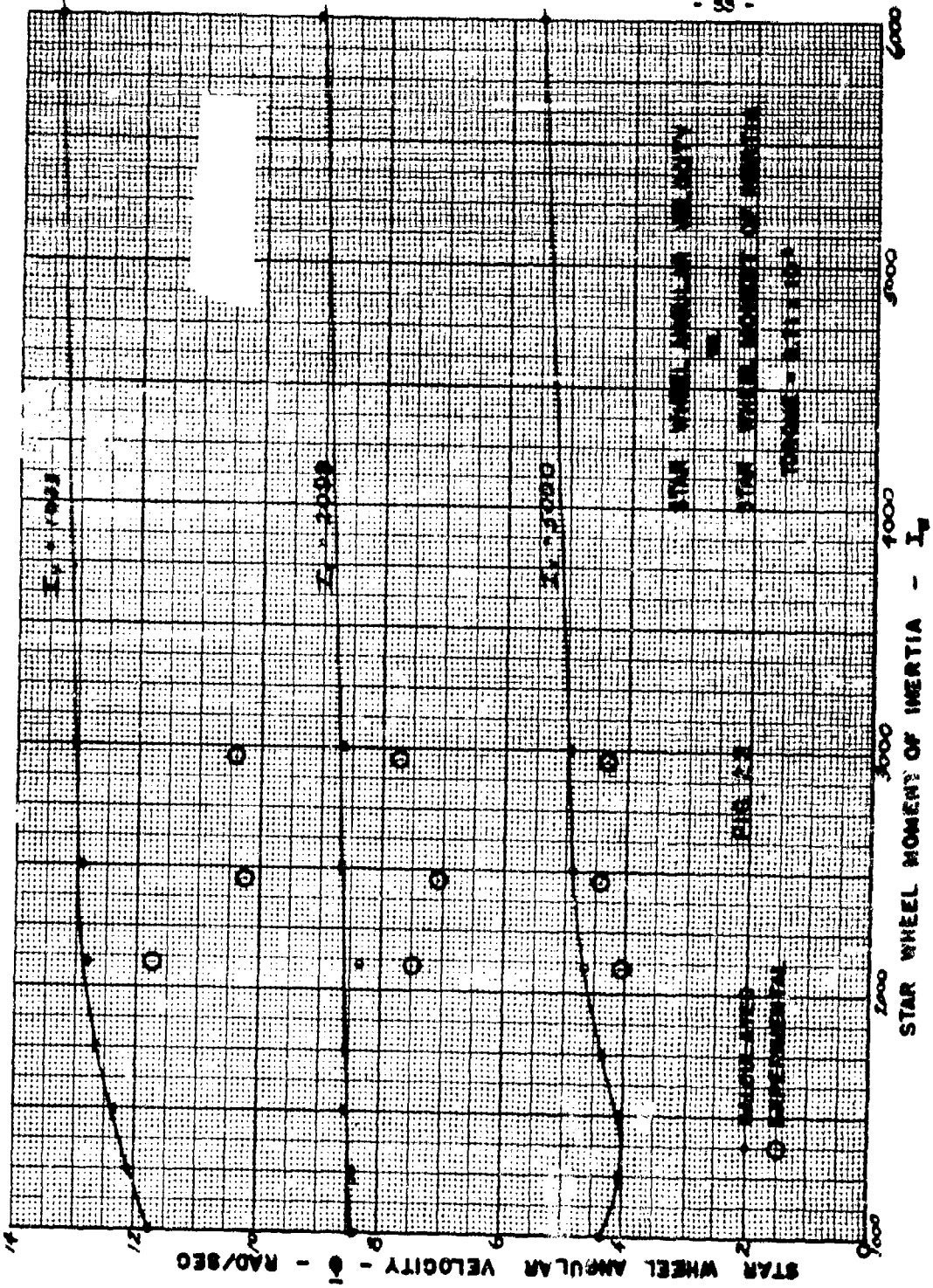
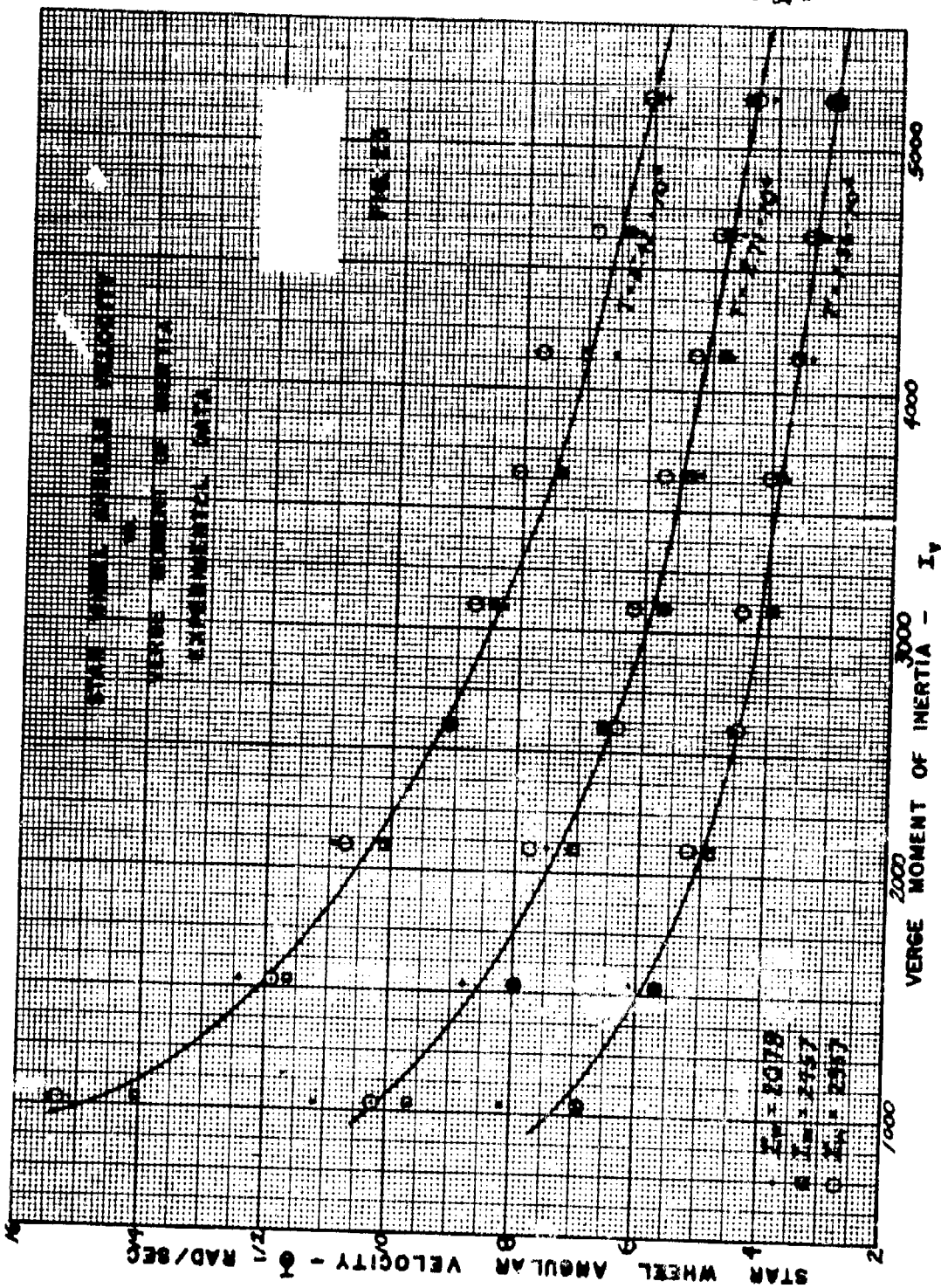


Fig-13



(F) EMPIRICAL EQUATION FOR TERMINAL VELOCITY

We are now prepared to derive an empirical equation which will predict  $\bar{\theta}$  for a given physical situation. It is clear from both theory and experiment that  $\bar{\theta}$ , for a verge-wheel combination of given shape and center spacing, can depend only upon three things; (1) applied torque  $\tau$ , (2) wheel moment of inertia  $I_w$ , (3) verge moment of inertia  $I_v$ .

We have found above that

$$\bar{\theta} \sim \tau^{.612} I_v^{-.112}$$

Dimensionally,  $I_w$  must enter this equation in such a manner that the right hand side of the equation has the dimensions  $1/\text{time}$ . The simplest possible way to accomplish this is to write

$$\bar{\theta} = A \tau^{.612} I_v^{-.112} I_w$$

which gives us correct dimensions for  $\bar{\theta}$ . Now A is a constant (or should be) which is dimensionless, being determined, as it is, only by the geometrical shapes and dimensions of the wheel-verge combination.

To check this equation we computed A for sixteen different values of  $\bar{\theta}$  and their corresponding values of  $\tau$ ,  $I_v$  and  $I_w$ . We found that

$$A = .231 \pm 1.3\%$$

as a mean value

Hence

$$\bar{\theta} = .231 \tau^{.612} I_v^{-.112} I_w$$

is the empirical equation predicting the terminal velocity for the particular wheel-verge combination under study.

We next repeated this procedure for experimental values of  $\bar{\theta}$ , using same cases as above. We now found that

$$A = .200 \pm 4\%$$

Here also, then, it seems to be time that our empirical equation will predict with reasonable accuracy the values of  $\bar{\theta}$  for given values of the other variables. The deviation in A only reflects, of course, the experimental variations among the determined values of  $\bar{\theta}$ . That this value of A is smaller is also to be expected, since the effect of friction, ignored in our theoretical work, will clearly decrease the values of  $\bar{\theta}$  below theoretical expectations.

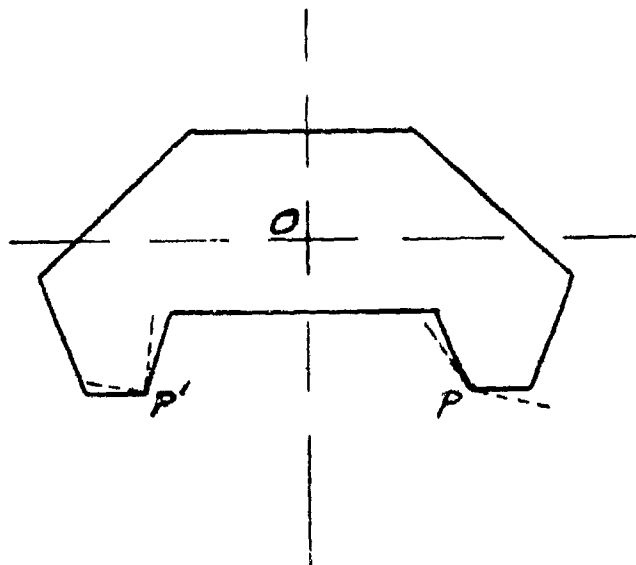
In practice it is more common to discuss delay time per star wheel revolution than it is to discuss terminal velocity. Hence we may rewrite our empirical equations as

$$T = B r^{-1/2} I_v^{.612} I_w^{-.112}$$

where  $T$  is time delay per revolution and  $B = \frac{2\pi}{A}$ .

(G) EFFECT OF PALLET FACE SLOPES UPON TERMINAL VELOCITY

This section of the report indicates certain preliminary results only. Reference to fig. 24 will indicate what changes were made in the pallet faces.



Points P and P' are kept in the same places with respect to O, the center of rotation of the verge.

FIG. 24

The angles at P and P' were increased or decreased. At P is shown approximately the "+12° Verge" in which each face of the verge was rotated outward 12°, giving a total increase in the angle at the corner of 24°. The same thing was done at P' of course.

The dotted lines at P' indicate how verge faces were rotated inward 12° each to make the "-12° Verge". The total decrease in angle at the corner is here 24°, and of course is done at both P and P'.

When one changes the slope of the pallet faces one is confronted with a completely new situation. It is necessary to return to the basic calculations, find how  $\alpha$  varies with  $\theta$ , and how  $u/v$  varies with  $\theta$ , and then recompute a whole new series of terminal velocities.

Such calculations have been carried out for the "+ 4° Verge" and the "-4° Verge", for a range of values of  $L_v$ . Single calculations for the "+ 12° Verge" and the "-12° Verge" have been computed.

Certain tentative conclusions may be drawn from this scanty data. As the angles at P and P' are decreased, terminal velocities tend to decrease, and as the angles are increased, terminal velocities tend to increase. Because of the geometrical factors involved, the "+ 12° Verge" and the "- 12° Verge" are limiting cases beyond which the apparatus jams for one reason or another.

More data will be acquired and a fuller discussion of the effect of slope of pallet faces on terminal velocity will be given later. In particular it is hoped that the effect of this factor upon the constant term A of the empirical equation might be found.

In closing this section it should be remembered that all work described above was carried out with the model in mind, none is directly applicable to the actual Lux clock mechanism without further discussion.

VII. EXPERIMENTAL METHODS. THE MODEL

(A) THE MODEL

Preliminary to extensive theoretical work on the operation of the mechanism, a model of the star wheel and verge was constructed of brass. The dimensions of this model were ten times those of the actual mechanism except for star wheel thickness and the size of the star wheel and verge shafts. The moments of inertia of both the model star wheel and verge were measured using a torsion pendulum, this data being given below. Since the theoretical work on the star wheel and verge motions involved moments of inertia, geometrical relationships of the star wheel teeth and the pallets of the verge, the fact that the star wheel thickness and the shafts were not to scale was of no consequence. The star wheel teeth and the verge pallets were constructed, scaled up ten times, according to the tolerances specified for the actual mechanism. To minimize the effects of friction, the star wheel and verge shafts were mounted in ball bearings. Various cylinders or disks of brass of known moment of inertia were made to be fastened by set screws to the verge and star wheel shafts so that effectively the verge or star wheel moment of inertia could be increased. Later in the course of the experimental work, a verge was made with removable pallets in order that a study might be made of the effect of the shape of the pallets on the terminal velocity of the star wheel. A picture of the completed model with the new verge incorporated is shown as Fig. 25. A torque was applied to the star wheel by hanging weights on a cord wrapped about the wooden driving pulley shown clearly in this photograph.

Since the theoretical results could be more readily checked experimentally using the model than by using the lux clock mechanism, the numerical values for moments of inertia and torque used in the theory are those that are applicable to the model. This information concerning the model is as follows:

Moments of Inertia:

Star wheel alone	1648 gm-cm <sup>2</sup>
Driving pulley on star wheel shaft	451 gm-cm <sup>2</sup>
Minimum star wheel moment of inertia used experimentally	2079 gm-cm <sup>2</sup>
Verge moment of inertia	1033 gm-cm <sup>2</sup>

By adding brass disks, the star wheel moment of inertia could be increased to the following values: (These include the moment of the wheel and the driving pulley.)

2457 gm-cm <sup>2</sup>
2957 gm-cm <sup>2</sup>
5957 gm-cm <sup>2</sup>

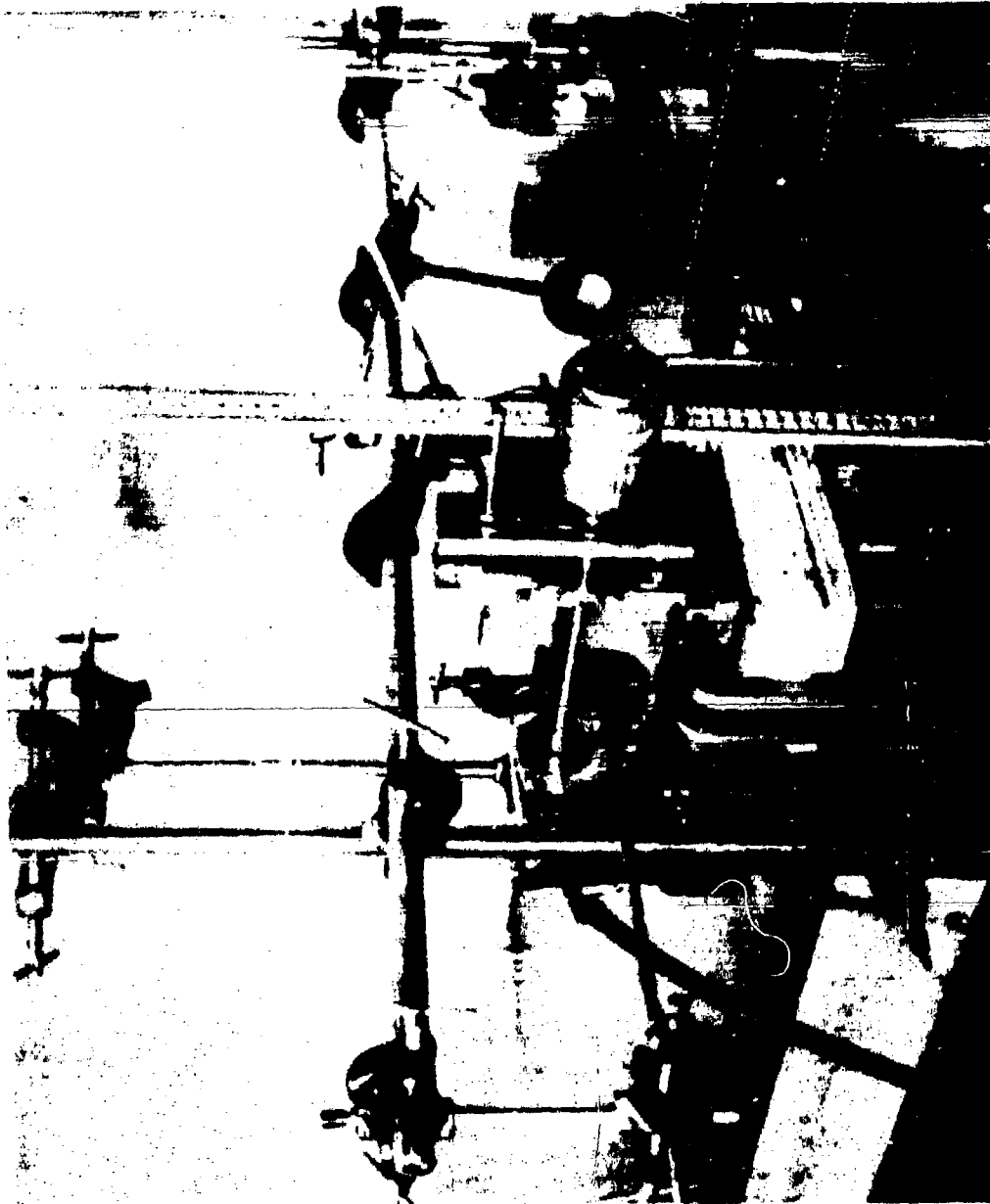


FIG. 25

Similarly by adding brass cylinders to the verge shaft the following values were obtained for total verge moment of inertia:

1533 gm-cm <sup>2</sup>	3098	4640
2098	3640	5205
2596	4140	

The radius of the driving pulley was 2.76 centimeters. A layout of the various discs and cylinders, as well as verge and starwheel is shown in Fig. 26.

#### (B) VERGE AND WHEEL POSITIONS AS FUNCTIONS OF TIME

A carbon potentiometer was connected across a battery. The potentiometer shaft was coupled to the verge shaft and connection made from the center terminal of the potentiometer (contact arm) to the vertical plates of the CRO. The grounded side of the CRO input was connected to the negative terminal of the battery. The horizontal sweep time of the oscilloscope could be varied continuously and was calibrated to within 5%. If the verge moved at constant velocity the trace should be a straight line whose slope is proportional to the velocity of the verge. Deviations from the linear trace indicate the nature of the verge motion, as plotted against time.

A wire wound potentiometer was coupled to the star wheel shaft and connections made as described above for the verge position as a function of time. The wire wound potentiometer was modified to allow 360° rotation. If the star wheel were to rotate at constant speed, the potential difference between the contact arm of the potentiometer and ground would produce a saw-tooth wave on the oscilloscope screen. The photographs representing the star wheel position as a function of time were obtained by turning up the oscilloscope gain and triggering the sweep at the beginning of a revolution of the potentiometer. Thus the photographed trace shows the position of the star wheel as a function of time for one cycle of the verge, the slope of the curve being proportional to velocity.

To obtain an oscilloscope trace that presented the relationship between star wheel position and time as a continuous curve, the apparatus shown by diagram Q in Fig. 27 was used. A disk with a sector cut in it was attached to the star wheel shaft so as to rotate in front of an arc shaped slit. A type 929 photocell was placed in a housing behind this arc shaped slit. Fig. 28 shows cathode follower circuit used with photo cell. If a light beam from a 22 c.p. source uniformly illuminates the portion of the sector disk in front of the photocell slit, a triangular pulse should be produced as the sector passes in front of the slit at constant angular velocity. This would occur if the light passing through the sector just fills the slit when the sector and slit coincide. If this condition is not met, the peak of the triangular pulse would be

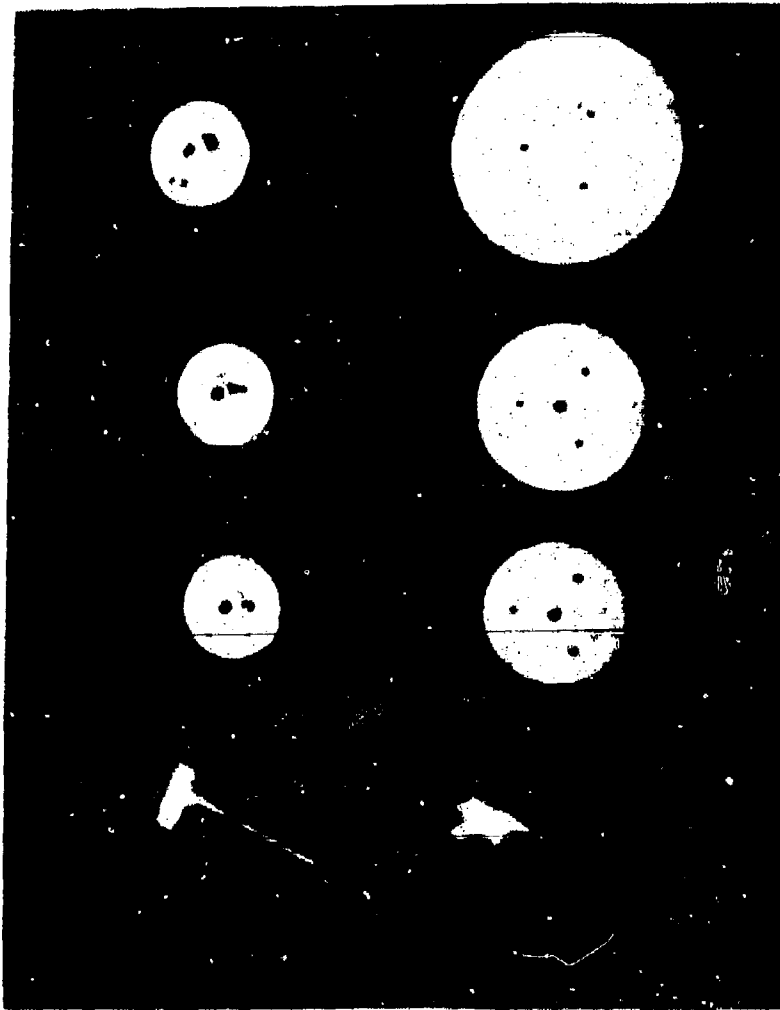


FIG-26

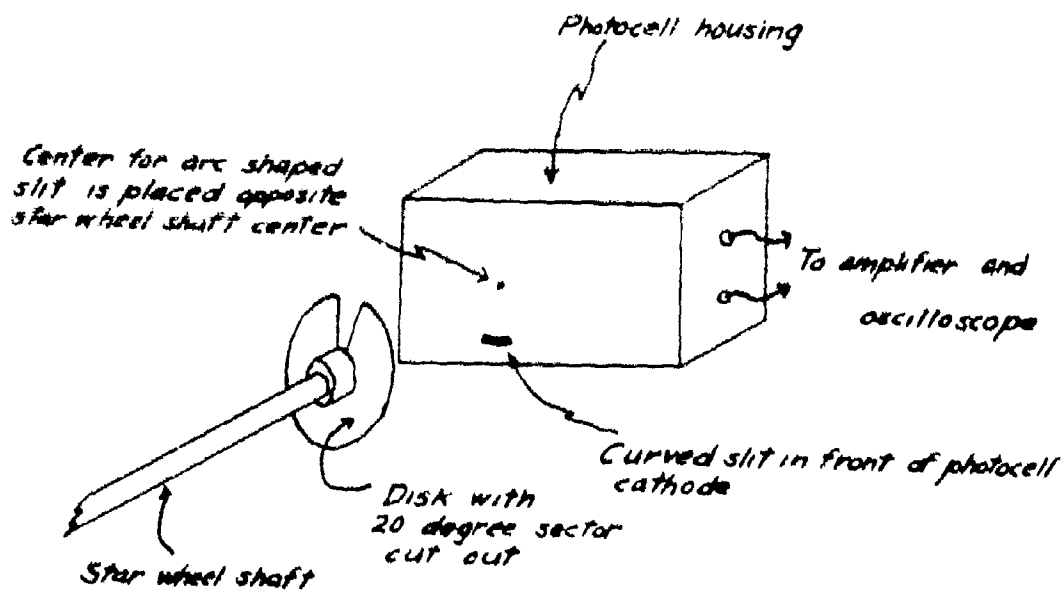


Fig. 27a

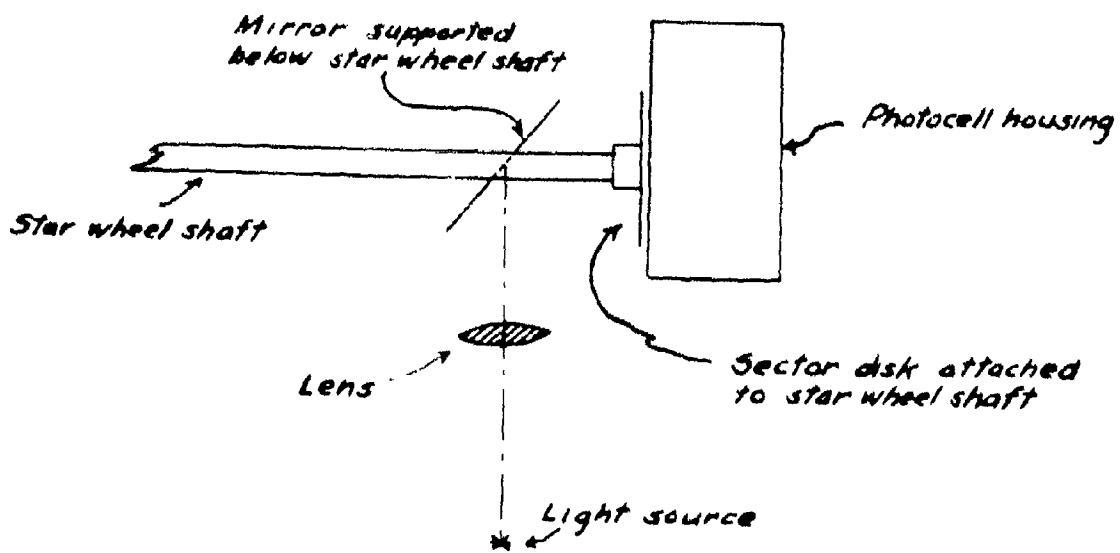


Fig. 27b

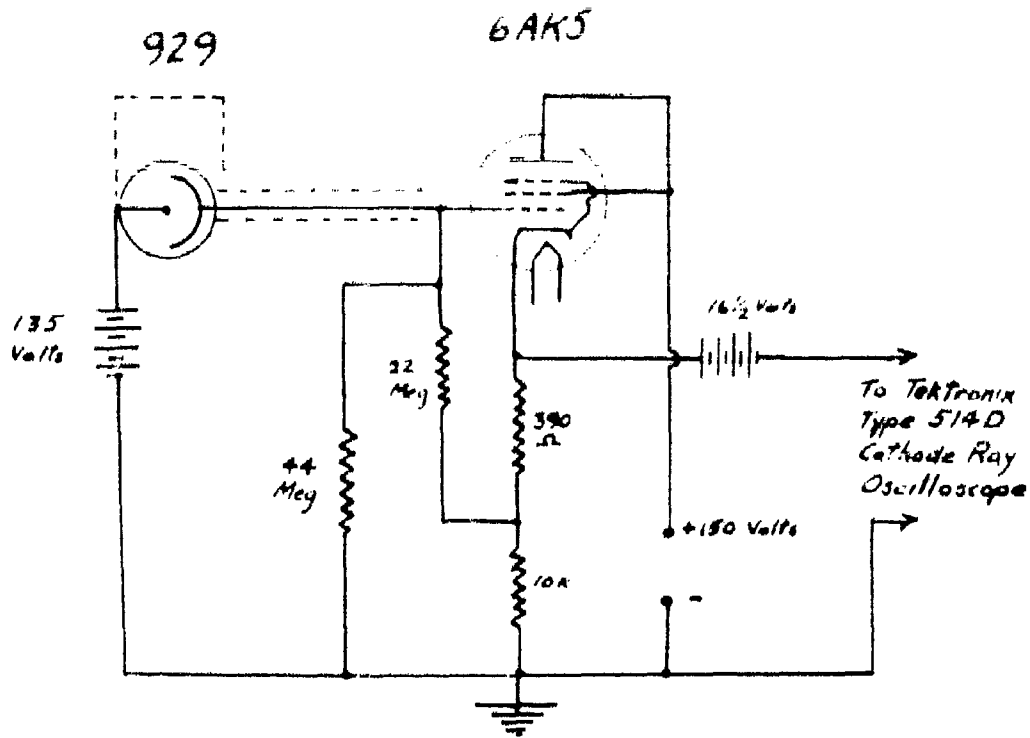


Fig. 28 Cathode follower and photocell circuit used in apparatus for determination of star wheel position as a function of time.

out off. The method used to insure that the CRO trace accurately represented the star wheel position as a function of time was as follows. The verge was removed and the star wheel rotated at constant speed by a pulley system from a motor. The light beam was then focussed on the sector so as to give a trace of constant slope on the oscilloscope screen. The sweep time of the oscillograph may be adjusted to show only that portion of the triangular pulse produced as the sector comes in line with the slit.



Fig. 29 shows the linear pulse when the wheel moves at uniform velocity (lower photograph).

The upper curve is the trace produced by the wheel in the case  $I_v = 2098 \text{ gm.cm.}^2$ ,  
 $I_w = 2079 \text{ gm.cm.}^2$ ,  
 $\gamma = 2.71 \times 10^6 \text{ dyne cm.}$

Fig- 29

Fig. 30 is a photograph of the apparatus as described above for the P. E. cell method.

### 3) VERGE MOTION AND EQUILIBRIUM CONDITIONS

A check was made on the number of cycles required for the model star wheel to reach equilibrium conditions. This was done by attaching a phosphor bronze wire to the verge and connecting the frame of the model to the ground of the CRO. Two phosphor bronze wires were arranged on opposite sides of the first wire so that as the verge oscillated, the center wire and one of the outside wires would act as a switch closing a circuit applying a potential to the CRO and producing a deflection. After a half cycle, the other outside wire and the center acted as a switch to apply a different and opposite potential to the CRO producing a different deflection in the opposite direction. If the deflections in successive cycles were equally spaced, terminal velocity of the star wheel had been obtained. The CRO sweep was manually triggered just before the model was allowed to start.

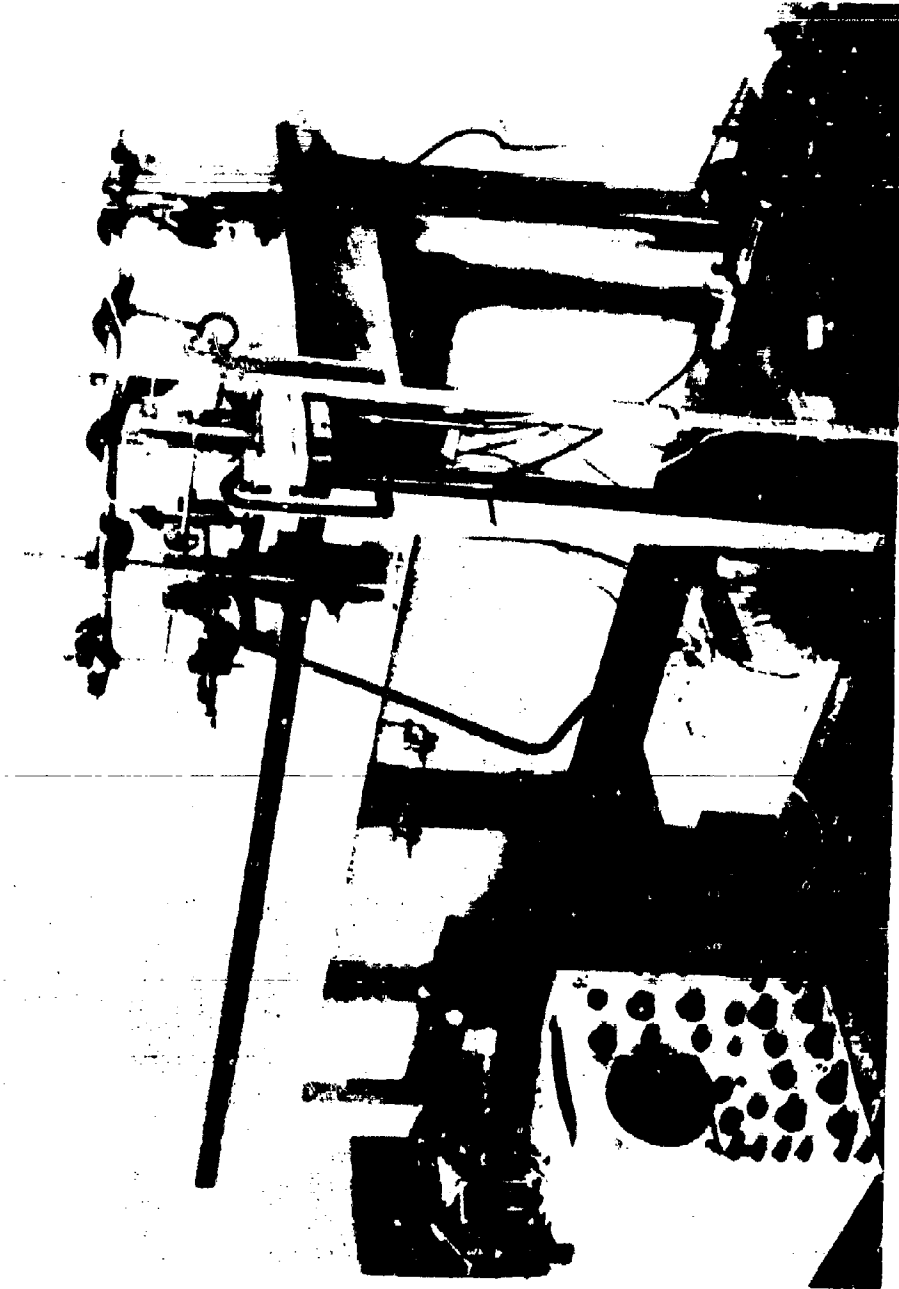


FIG. 30

(D) TERMINAL VELOCITY MEASUREMENTS

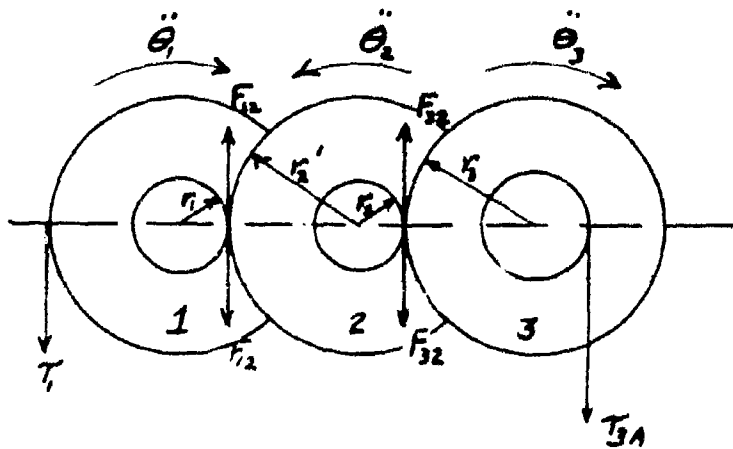
Various loads were suspended by a string attached to the wooden driving pulley, thus securing a range of driving torques. Terminal velocities were determined from measurements of time required for the loads to fall a distance of 140 cm. Many such measurements were made over a range of wheel moments and verge moments.

In all of the above mentioned measurements of terminal velocity the driving load and wheel were started from rest and no correction was made for the time to reach terminal velocity. The correction was found to be negligible since the wheel made about eight revolutions in the measured time and calculations showed that equilibrium was reached in about one-seventh of a revolution.

VIII. LUX CLOCK MECHANISM: DATA, RESULTS, EXPERIMENT

(A) THE APPLICATION OF THEORY TO THE LUX CLOCK MECHANISM.

In reviewing our theory as applied to the model we will remember that the star wheel was considered to be free except for the constant applied torque and the reaction torque applied to it by the verge. In the actual mechanism however, there is clearly an interaction between the star wheel and the remainder of the gear train. This could possibly result in a considerably increased effective moment of inertia for the star wheel. Thus, we have considered that wheel moment plays a small role in determining  $\theta$ , but it seems necessary to investigate the above situation regardless.



*Gear train of Lux clock mechanism*

FIG. 30

Fig. 30 is a schematic diagram of the gear train of the Lux clock mechanism. Gear # 1 is the star wheel, and Gear #3 is the first gear in the train. Some clock mechanisms have two intermediate gears rather than one. We shall adapt our result to a general case, so that the situation pictured is sufficient for our purposes.

$T_{3A}$  is a schematic representation of the torque applied by the spring to the first gear wheel. Similarly  $T_1$  is a schematic representation of the torque applied by

the verge to the star wheel. The other symbols and vectors are self-evident. The moments of inertia of the three gear wheels are  $I_1$ ,  $I_2$ , and  $I_3$  respectively.

Writing differential equations of motion for three gears gives

$$(1) F_{12} r_1 - T_1 = I_1 \ddot{\theta}_1$$

$$(2) - F_{12} + F_{32} - I_2 \ddot{\theta}_2$$

$$(3) T_{3A} - F_{32} = I_3 \ddot{\theta}_3$$

Solving simultaneously gives

$$\frac{T_{3A}}{M_{21} M_{32}} - T_1 = \left[ I_1 + \frac{I_2}{M_{21}^2} + \frac{I_3}{M_{32}^2 M_{21}^2} \right] \ddot{\theta},$$

where  $M_{21} = \frac{r_2}{r_1}$ ,  $M_{32} = \frac{r_3}{r_2}$ , the mechanical advantages.

$\frac{T_{3A}}{M_{21} M_{32}}$  is nothing but the torque applied to the star wheel by the spring and gear train, and is the torque called  $T$  in preceding work. The term in brackets is the effective moment of the star wheel. Now in the mechanism  $M_{21} = 5$ ,  $M_{32} = 7$  approximately. Clearly then, the second and third terms in the bracket can be neglected since  $I_2$ ,  $I_3$  are approximately the size of  $I_1$ . Quite clearly this situation could be readily generalized to a number of gears with the same conclusion.

As far as the effect of the gear train on the wheel is concerned, the theory for the model may be applied unchanged to the clock mechanism.

#### (B) COMPARISON OF EXPERIMENTAL AND THEORETICAL MOTIONS

It has already been noted that the model used was scaled up 10 times, which results in scaling up the moments of inertia by  $10^5$ . If the velocities attained in the model were to be the same order of magnitude as those attained by the actual mechanism, it would be necessary to scale up the applied torques by a factor  $10^5$  also. Rough calculations show that the torques actually applied in the model were scaled up only  $10^3$  times. Hence the velocities actually attained in the model were some 100 times smaller than those found in the mechanism.

Now we ask this question. Will our failure to use large torques in the model result in theoretical predictions, theoretical curves in particular, which will not be found experimentally? The answer is yes, but not basically because of a break down in theoretical

calculations. Recall that one of our basic assumptions was that the time during which a collision takes place is infinitesimally small, so that the applied torque was ineffective during collision. We know that this is not true. As the torque increases such a supposition leads to results less trust worthy. For example, suppose that our theory predicts that the instantaneous collision should result in a reversal of direction of the star wheel, as always does happen when  $I_v$  is two or more times larger than  $I_w$ . In actuality, this collision is dragged out over several milliseconds so that the change in velocity mentioned above does not take place instantaneously. Rather, the applied torque acting during this interval prevents the reversal predicted by theory. The larger the applied torque, the greater its effectiveness in preventing the changes in velocity predicted by theory.

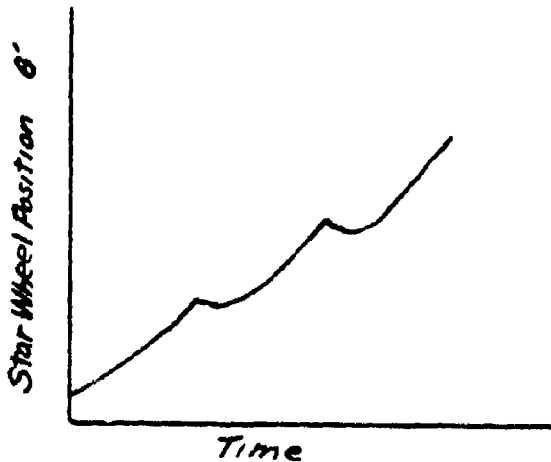


Fig. 31

Fig. 31 is a sketch of the kind of curve theory predicts for the case when  $I_v > 3I_w$ , showing that the wheel backs up at each collision.



Fig. 32

Fig. 32 is an experimental record of the curve for the clock mechanism for the same case. A comparison of the curves indicates how the physical situation described above alters the behaviour of the star wheel. The "backing up" tendency of the wheel is smoothed out as the result of the effect of the applied driving torque.

Fig. 32 is a photograph of a CRO trace obtained for the Lux clock mechanism using a photo cell as described in Section VII for the model. The Lux clock mechanism was disassembled and matching holes drilled through the plate of the mechanism that support the gear train and through the star wheel itself. Then small pieces of aluminum foil were glued with Duco cement around the edges of the hole in the star wheel so as to form an arc shaped slit in the star wheel. Aluminum foil was similarly used to form an arc shaped slit in one of the base plates of the mechanism. After reassembling the mechanism, it was mounted in front of the 929 photo cell. A light beam was focussed on the slit as shown in the photograph (Fig. 33). To be sure that the traces obtained on the oscilloscope screen presented the relationship between star wheel position and time, the apparatus was run at constant speed with the verge removed. To run the mechanism at constant speed, the spring operated driving gear was disengaged and an auxiliary pulley driven gear used to drive the mechanism.

#### (C) PHYSICAL CONSTANTS OF THE CLOCK MECHANISM

Lux clocks having nominal times of 1/2, 1, 1-1/2, 5, and 10 sec were used to obtain data on driving spring torque, mechanical advantage of gear train, static star wheel torque, terminal velocities, limits of angular motion of verge, number of cycles of verge for star wheel to reach terminal velocity, and moments of inertia of star wheel and verge.

Terminal velocity of the star wheel was measured by counting the number of revolutions of the star wheel and estimating fractions of revolutions in the complete run of the clock. This number was divided by the time required for the complete run as measured by the average of ten time measurements made with an electric seconds timer.

Terminal velocity of the star wheel was also obtained by use of a photo cell receiving light reflected from a mirror on the star wheel at each revolution. The photo-cell pulse was fed to CRO and the calibrated sweep time was used to calculate the terminal velocity. This method was used to check the other method which was normally used.

The spring torque in each clock was measured by a lever arm and weight arrangement. Measurements were made with gear train disengaged and engaged with the verge out of the clock.

Static star wheel torque was measured by a lever arm and weight arrangement using the hub on the star wheel as the cylinder on which to wind the thread from which the weight hung.



FIG 33

The mechanical advantage of the two types of gear trains used in the 1/2, 1, 1-1/2, 5 and 10 sec clocks was calculated from the number of teeth in each gear.

Moments of inertia of star wheel and verge were determined using a silk thread as the suspension and applying the torsion pendulum method. These values checked well with those of the model when scaled down by the factor of 10<sup>5</sup>.

No data gathered as outlined above is recorded here. It will be referred to as needed later.

(D) NUMBER OF CYCLES PRECEDING EQUILIBRIUM

A beam of light falling on a photo cell was interrupted by the teeth of the rotating star wheel. The resulting signal on the screen of a CRO was photographed and shown as fig. 34.



The distance between adjacent peaks of the trace indicate time intervals. The photograph shows clearly that an equilibrium condition is reached in approximately 3 cycles. Apparatus starts from rest at left side of trace.

Fig. 34

(E) EMPIRICAL EQUATION FOR TERMINAL VELOCITIES

Recalling the empirical equation derived for the model, we ask if a similar equation can be found for the actual mechanism. In order to check such an equation, we need to know the moments of inertia of star wheel and verge. Likewise the angular speed could be determined. The most difficulty is met when we attempt to measure the torque. Inspection of the various models of the mechanism indicate that the same spring is used in each. However there is considerable variation in the measured values of the torque applied to the star wheel. Quite clearly friction between spring coils, between gear teeth, and at shafts all contribute differing amounts of resistive torque. It is not at all surprising that our experimental measurements should vary widely.

If one now attempts to set up an empirical equation of the form

$$\bar{\theta} = A T^{.612} I_v^{.112} I_w$$

one must use the experimental values of  $\bar{\theta}$ ,  $\tau$  etc. in order to determine  $A$ . If this is done we find

$$A = .18 \pm .018 = .18 \pm 10\%$$

approximately. How much of the angular deviation is caused by breakdown of theory is problematical. The data used would suggest that the more important reason for the large deviation lies in the lack of consistency in experimental data used to determine  $A$ . No substantiation of the following statement can be made, but it is probably true that if better experimental data were available the empirical formula would predict much more closely the true values of  $\bar{\theta}$ .

BEST AVAILABLE COPY

one must use the experimental values of  $\bar{\theta}$ ,  $\bar{T}$  etc. in order to determine  $A$ . If this is done we find

$$A = .18 \pm .018 = .18 \pm 10\%$$

approximately. How much of the angular deviation is caused by breakdown of theory is problematical. The data used would suggest that the more important reason for the large deviation lies in the lack of consistency in experimental data used to determine  $A$ . No substantiation of the following statement can be made, but it is probably true that if better experimental data were available the empirical formula would predict much more closely the true values of  $\bar{\theta}$ .

**BEST AVAILABLE COPY**

APPENDIX A

COMPLETE SOLUTION FOR THE MOTION OF THE SYSTEM

This calculation is begun with the assumption that the star wheel and verge are stationary with the verge in the equilibrium position and the star wheel in leading contact. The following symbols will be used throughout.

$\theta_0$  - Angular position of radius vector to tip of star wheel tooth at leading contact with verge in equilibrium position, measured in radians from the center line of star wheel and verge, positive angles being measured clockwise.

$\theta_1$  - Angular position of radius vector to tip of star wheel tooth at last contact leading.

$\theta_2$  - Angular position of radius vector to tip of star wheel tooth at trailing collision.

$$\theta_3 = \theta_2$$

$\theta_4$  - Angular position of radius vector to tip of star wheel tooth at last contact trailing.

$\theta_5$  - Angular position of radius vector to tip of star wheel tooth at leading collision.

$$\theta_6 = \theta_5$$

$\theta_{3A}$  - Angular position of radius vector to tip of star wheel tooth in trailing contact at the instant the star wheel resumes rotation in the positive sense if the star wheel has been caused to reverse direction upon collision with the verge.

$\theta_{3B}$  - Angular position of radius vector to tip of star wheel tooth in trailing contact when star wheel returns to the position of trailing collision with a positive velocity.  $\theta_{3B}$  is equal to  $\theta_3$  and appears only in the case where the trailing collision causes a reversal of the star wheel.

$\theta_{6A}$  - Angular position of radius vector to tip of star wheel tooth in leading contact at the instant the star wheel resumes rotation in the positive sense after a leading collision which has caused reversal.

$\theta_{6B}$  - Angular position of radius vector to tip of star wheel tooth in leading contact when star wheel returns to the position of leading collision with a positive velocity and is equal to  $\theta_6$ .

$\alpha_2$  - Angular position of the verge at trailing collision measured in radians from the equilibrium position of the verge, positive angles being measured in a counterclockwise direction.

$\alpha_3$  - Angular position of the verge at leading collision measured in the same manner as  $\alpha_2$ .

$\dot{\theta}_1$  - Angular velocity of star wheel at last contact leading, clockwise velocities being positive.

$\dot{\theta}_2$  - Angular velocity of star wheel just prior to trailing collision.

$\dot{\theta}_3$  - Angular velocity of star wheel immediately following trailing collision.

$\dot{\theta}_4$  - Angular velocity of star wheel at last contact trailing.

$\dot{\theta}_5$  - Angular velocity of star wheel just prior to leading collision.

$\dot{\theta}_6$  - Angular velocity of star wheel immediately after leading collision.

$\dot{\theta}_{3B}$  - Angular velocity of star wheel at  $\theta_{3B}$ .

$\dot{\theta}_{6B}$  - Angular velocity of star wheel at  $\theta_{6B}$ .

$\dot{\alpha}_1$  - Angular velocity of verge at last contact leading, positive verge velocities being measured in a counterclockwise direction.

$\dot{\alpha}_2 = \dot{\alpha}_1$  - Angular velocity of verge just prior to trailing collision.

$\dot{\alpha}_3$  - Angular velocity of verge immediately following trailing collision.

$\dot{\alpha}_{3B}$  - Angular velocity of verge corresponding to the star wheel velocity  $\dot{\theta}_{3B}$ .

$\dot{\alpha}_4$  - Angular velocity of verge at last contact trailing.

$\dot{\alpha}_5$  - Angular velocity of verge immediately prior to leading collision.

$\dot{\alpha}_6$  - Angular velocity of verge immediately after leading collision.

$\dot{\alpha}_{6B}$  - Angular velocity of verge corresponding to the star wheel velocity  $\dot{\theta}_{6B}$ .

$K, K', A, B, A', B', V, V'$  - Constants determined from the space relationship curves.

$T$  - Driving torque (assumed constant) applied to the star wheel.

$I_V$  - Moment of inertia of the verge.

$I_W$  - Moment of inertia of the verge.

$\theta_K$  - The angle in radians between the radius vector to the tip of a tooth at leading contact to the radius vector to the tip of the tooth which makes the next trailing contact (in this case, five tooth spaces) and is always considered positive.

$\theta_{K'}$  - The angle in radians between the radius vector to the tip of a tooth at trailing contact to the radius vector to the tip of the tooth which makes the next leading contact (in this case, four tooth spaces) and is always considered positive.

The velocities of the star wheel and verge at the various points in the first cycle are calculated from the following equations:

$$\dot{\theta}_1 = \frac{2T}{A} \ln \frac{AB_1 + B}{AB_0 + B} \quad (1)$$

$$\dot{\alpha}_1 = V\dot{\theta}_1 \quad (2)$$

After last contact leading, the verge continues to turn with a constant angular velocity equal to  $\dot{\alpha}_1$ , while the star wheel is accelerated by the driving torque. The positions of star wheel and verge at trailing collision must now be determined. One method of accomplishing this is to assume a value and calculate the time lapse between last contact leading and trailing collision from the equation:

$$t = \frac{\alpha_2 - \alpha_1}{\dot{\alpha}_1} \quad (3)$$

The corresponding value is calculated:

$$\theta_2 = \frac{1}{2} \frac{T}{I_W} t^2 + \dot{\theta}_1 t + (\theta_1 - \theta_K) \quad (4)$$

This point ( $\alpha_2, \theta_2$ ) is located on the graph of  $\alpha$  vs.  $\theta$  and successive values of  $\alpha_2$  are chosen and the procedure repeated until the point lies on the curve.

The star wheel and verge velocities just prior to trailing collision are calculated from the following:

$$\dot{\theta}_2 = \frac{Y}{I_w} t + \dot{\theta}_1 \quad (5)$$

$$\dot{\alpha}_2 = \dot{\alpha}_1 \quad (6)$$

Star wheel and verge velocities immediately following trailing collision are given by the equations:

$$\dot{\theta}_3 = \frac{I_w \dot{\theta}_2 - K' I_v \dot{\alpha}_2}{I_w - K' I_v Y'} \quad (7)$$

$$\dot{\alpha}_3 = Y' \dot{\theta}_3 \quad (8)$$

In the event that the value of  $\dot{\theta}_3$  as determined from equation (7) is negative a reversal of the direction of star wheel motion occurs and it becomes necessary to determine the position at which the star wheel comes to rest as follows:

$$\theta_{3A} = \frac{A' \dot{\theta}_3 + B'}{A'} e^{-\frac{A' \dot{\theta}_3^2}{2T}} - \frac{B'}{A'} \quad (9)$$

Following this, the wheel moves in a positive direction and arrives at the position at which collision occurred with a velocity:

$$\dot{\theta}_{3B} = \frac{2T}{A'} \ln \frac{A' \theta_{3B} + B'}{A' \theta_{3A} + B'} \quad (10)$$

This velocity is equal to minus  $\dot{\theta}_3$ .

The wheel drives the verge until the position of last contact trailing is reached, at which point the velocities are determined as follows:

$$\dot{\theta}_4 = \dot{\theta}_{3B} + \frac{2T}{K'} \ln \frac{A' \theta_4 + B'}{A' \theta_{3B} + B'} \quad (11)$$

$$\dot{\alpha}_4 = Y' \dot{\theta}_4 \quad (12)$$

If the velocity  $\dot{\theta}_3$  as determined by equation (7) is positive, equations (9) and (10) are not used and  $\theta_{3B}$  and  $\dot{\theta}_{3B}$  in equation (11) are replaced, respectively, by  $\theta_3$  and  $\dot{\theta}_3$ .

Following last contact trailing the verge continues to rotate at a constant angular velocity equal to  $\dot{\alpha}_4$  while the wheel is accelerated by the driving torque.

The point of leading collision must now be determined as in the case of trailing collision previously discussed. A value of  $\alpha_5$  is chosen and the time lapse between last contact trailing and leading collision is calculated by the equation:

$$t' = \frac{\alpha_5 - \alpha_4}{\dot{\alpha}_4} \quad (13)$$

$$\theta_5 = \frac{1}{2} \frac{\tau}{I_w} t'^2 + \dot{\theta}_4 t' + (\theta_4 + \theta_K) \quad (14)$$

As before,  $t'$  is located on the graph of  $\alpha$  vs.  $\theta$  and the value of  $\alpha_5$  is varied until the point lies on the curve.

The star wheel and verge velocities just prior to leading collision may then be determined as follows:

$$\dot{\theta}_5 = \dot{\theta}_4 + \frac{\tau}{I_w} t' \quad (15)$$

$$\dot{\alpha}_5 = \dot{\alpha}_4 \quad (16)$$

Velocities immediately following leading collision are then calculated by the equations:

$$\dot{\theta}_6 = \frac{I_w \dot{\theta}_5 + K I_v \dot{\alpha}_5}{I_w + K I_v} \quad (17)$$

$$\dot{\alpha}_6 = \tau \dot{\theta}_6 \quad (18)$$

As in the trailing collision, if the value of  $\theta_6$  as given by equations (17) is negative, the position at which the star wheel comes to rest is determined from the following:

$$\theta_{6A} = \frac{A \theta_6 + B}{A} = \frac{-A \theta_6^2}{2\tau} - \frac{B}{A} \quad (19)$$

The velocity reached by the star wheel upon arrival at the position of collision is equal to minimum  $\dot{\theta}_6$  and may be checked by the following:

$$\dot{\theta}_{6B} = \frac{2\tau}{A} \ln \frac{A \theta_{6B} + B}{A \theta_{6A} + B} \quad (20)$$

$$\dot{\alpha}_{6B} = \tau \dot{\theta}_{6B} \quad (21)$$

This completes what is considered to be the first cycle of verge motion. As in the case of trailing collision, equations (19), (20) and (21) are used only when equation (17) gives a negative value of  $\theta_6$ .

To calculate the velocities at the various points in the second cycle, one proceeds as follows. The star wheel velocity at last contact leading is determined from the following equation:

$$\dot{\theta}_1^2 = \dot{\theta}_6^2 + \frac{EY}{A} \ln \frac{A\theta_1 + B}{A\theta_6 + B} \quad (22)$$

and the corresponding verge velocity is:

$$\dot{\alpha}_1 = Y \dot{\theta}_1 \quad (23)$$

From this point on, the calculation proceeds exactly as indicated in the first cycle, and each subsequent cycle follows the pattern of the second cycle. When the point is reached at which each velocity calculated for a cycle is the same as that obtained in the preceding cycle, the star wheel is considered to have reached a constant average velocity. It is worth noting that, for all cases considered up to the present time, this has occurred by the fourth cycle.

After the system reaches a constant average velocity the star wheel and verge velocities at the various points in the cycle are plotted against angular rotation of the star wheel. A convenient scale is obtained by considering the star wheel to be in the reference or zero position at the position of leading collision. In moving from the position of leading collision to the position of last contact leading, the star wheel must turn through an angle equal to the difference between  $\theta_6$  and  $\theta_1$ . The velocities of star wheel and verge at last contact leading are plotted at:

$$\theta'_1 = \theta_1 - \theta_6 \quad (24)$$

Since the angle  $\theta_1$  at last contact leading is referred to the tooth in leading contact and the angle  $\theta_2$  at trailing collision is referred to a different tooth at an angle  $\theta_K$  from the tooth in leading contact, the velocities  $\dot{\alpha}'_2$  and  $\dot{\theta}'_2$  are plotted at a point:

$$\theta'_2 = \theta'_1 + (\theta_K - \theta_1 + \theta_2) \quad (25)$$

Plotting points for subsequent velocities are determined as follows:

$$\theta'_3 = \theta'_2 \quad (26)$$

$$\theta'_{3A} = \theta'_3 - (\theta_3 - \theta_{3A}) \quad (27)$$

$$\theta'_{3B} = \theta'_3 \quad (28)$$

$$\theta'_4 = \theta'_3 + (\theta_4 - \theta_3) \quad (29)$$

$$\theta_3' = \theta_4' + \theta_3 - \theta_K' - \theta_4 \quad (30)$$

$$\theta_2' = \theta_5' \quad (31)$$

$$\theta_{6A}' = \theta_6' - (\theta_6 - \theta_{6A}) \quad (32)$$

$$\theta_{6B}' = \theta_6 \quad (33)$$

As many intermediate points as necessary to draw the curve are calculated as follows. In the region from the origin to  $\theta_1'$ , intermediate points a distance  $\Delta\theta$  from the origin are determined from the equation

$$\dot{\theta}^2 = \dot{\theta}_0^2 + \frac{2T}{A} \ln \frac{A(\theta_0 + \Delta\theta) + B}{A\theta_0 + B} \quad (34)$$

In the region from  $\theta_1'$  to  $\theta_2'$ , intermediate points  $\theta_1' + \Delta\theta$  are given by:

$$\dot{\theta}^2 = \dot{\theta}_1^2 + \frac{2T}{w} \Delta\theta \quad (35)$$

In the region from  $\theta_3'$  to  $\theta_4$  intermediate points at  $\theta_3' + \Delta\theta$  are given by:

$$\dot{\theta}^2 = \dot{\theta}_3^2 + \frac{2T}{A'} \ln \frac{A'(\theta_3 + \Delta\theta) + B'}{A'\theta_3 + B'} \quad (36)$$

and in the region from  $\theta_4'$  to  $\theta_5'$ , intermediate points at  $\theta_4' + \Delta\theta$  are calculated from the equation:

$$\dot{\theta}^2 = \dot{\theta}_4^2 + \frac{2T}{I_w} \Delta\theta \quad (37)$$

Under the condition that the star wheel is reversed following a trailing collision, intermediate points in the region  $\theta_3'$  to  $\theta_{3A}'$  to  $\theta_{3B}'$  an interval  $\Delta\theta$  from  $\theta_{3A}'$  may be determined from the following:

$$\dot{\theta}^2 = \frac{2T}{A} \ln \frac{A'(\theta_{3A}' + \Delta\theta) + B'}{A'\theta_{3A}' + B'} \quad (38)$$

In this case the positive and negative roots are both used, the positive root yielding a point on the curve between  $\theta_{3A}'$  and  $\theta_{3B}'$  and the negative root a point between  $\theta_3'$  and  $\theta_{3A}'$ .

If the leading collision causes a reversal of the star wheel, points between  $\theta_6'$ ,  $\theta_{6A}'$  and  $\theta_{6B}'$  a distance  $\Delta\theta$  from  $\theta_{6A}'$  can be calculated in a similar manner from the equation:

$$\dot{\theta}^2 = \frac{2T}{A} \ln \frac{A(\theta_{6A}' + \Delta\theta) + B}{A\theta_{6A}' + B} \quad (39)$$

APPENDIX B

SHORT METHOD SOLUTION FOR THE MOTION OF THE SYSTEM

It is readily observed that the calculation of star wheel velocity by the method just outlined is a slow and tedious task particularly when it is necessary to calculate this velocity for a number of verge and star wheel moments and torques. In performing these calculations by the long method, it will be noted that, for star wheels and verge combinations with the same shaped surfaces, the verge and star wheel angles at trailing collision,  $\theta_2$  and  $\theta_3$ , and the corresponding angles at leading collision,  $\theta_5$  and  $\theta_6$ , are very nearly constant after terminal velocity is reached. These values are found to be nearly constant irrespective of the torque and of the verge and star wheel moments of inertia. Assuming them to be constant leads to a less laborious method of calculation of the average velocity of the star wheel. This method of calculation is outlined below.

Once the values of  $\theta_2$  and  $\theta_5$  are established by the previous method of calculation, the following constants are evaluated.

$$C_1 = \frac{2T}{X} \ln \frac{A \theta_1 + B}{A \theta_5 + B} \quad (40)$$

$$C_2 = \frac{2T}{I_w} (\theta_K - \theta_1 + \theta_2) \quad (41)$$

$$C_3 = -K' I_v \dot{\gamma} \quad (42)$$

$$C_4 = I_w - K' I_v \dot{\gamma}' \quad (43)$$

$$C_5 = \frac{2T}{A'} \ln \frac{A' \theta_4 + B'}{A' \theta_2 + B'} \quad (44)$$

$$C_6 = \frac{2T}{I_w} (\theta_5 - \theta_{K'} - \theta_4) \quad (45)$$

$$C_7 = K I_v \dot{\gamma}' \quad (46)$$

$$C_8 = I_w + K I_v \dot{\gamma}' \quad (47)$$

Now a value of  $\dot{\theta}_6$ , the star wheel velocity immediately following leading collision, is assumed and the velocities at subsequent points in the cycle are calculated from the following:

$$\dot{\theta}_1^2 = \dot{\theta}_5^2 + C_1$$

$$\dot{\theta}_2^2 = \dot{\theta}_1^2 + C_2$$

$$\dot{\theta}_3 = \frac{C_3 \dot{\theta}_1 + I_w \dot{\theta}_2}{C_4}$$

$$\dot{\theta}_4^2 = \dot{\theta}_3^2 + C_5$$

$$\dot{\theta}_5^2 = \dot{\theta}_4^2 + C_6$$

$$\dot{\theta}_6 = \frac{C_7 \dot{\theta}_4 + I_w \dot{\theta}_5}{C_8}$$

In all probability the value of  $\theta_5$  so obtained will not agree with the value assumed. Using the new value of  $\theta_5$  as the initial condition and repeating the process will in most cases yield a closed cycle very quickly.

Following this, the necessary intermediate points to plot a curve of star wheel velocity versus star wheel angular displacement are calculated as before, and the average velocity of the star wheel is determined as previously indicated.